A Novel Analytical Model of Solute Transport in an Aquifer-Aquitard System with Mixing Processes in the Reservoirs

Wenguang Shi
China University of Geosciences
Wang Quanrong (wangqr@cug.edu.cn)
China University of Geosciences https://orcid.org/0000-0002-6560-6340

Research Article

Keywords: Solute transport, Vertical dispersion, Aquifer-aquitard system, Parameter estimation

Posted Date: January 6th, 2022

DOI: https://doi.org/10.21203/rs.3.rs-1019431/v1

Title page

A Novel Analytical Model of Solute Transport in an Aquifer-aquitard System with Mixing Processes in the Reservoirs

Wenguang Shi[1] and Quanrong Wang[1, 2*]

[1]School of Environmental Studies, China University of Geosciences, 388 Lumo Road, Wuhan 430074, China

[2]State Environmental Protection Key Laboratory of Source Apportionment and Control of Aquatic Pollution, Ministry of Ecology and Environment, 388 Lumo Road, Wuhan 430074, China

Corresponding author: Quanrong Wang (wangqr@cug.edu.cn)

Competing interests statement: Declaration of interest: "none"

Ethics approval and consent to participate: "Not applicable"

Consent for publication: "Not applicable"

Availability of data and materials: The datasets used and/or analyzed during the current study are available from the corresponding author on reasonable request.

Funding: "No funds, grants, or other support was received"

Authors' contributions:

Conceptualization, Writing - review & editing, Supervision [**Quanrong Wang**], Methodology, Writing original draft, derivation, code, Formal analysis [**Wenguang Shi**]

A Novel Analytical Model of Solute Transport in an Aquifer-aquitard System with Mixing Processes in the Reservoirs

Wenguang Shi[1] and Quanrong Wang[1, 2*]

[1]School of Environmental Studies, China University of Geosciences, 388 Lumo Road, Wuhan 430074, China

[2]State Environmental Protection Key Laboratory of Source Apportionment and Control of Aquatic Pollution, Ministry of Ecology and Environment, 388 Lumo Road, Wuhan 430074, China

Corresponding author: Quanrong Wang (wangqr@cug.edu.cn)

Highlights:

1. A novel MIM analytical model of solute transport is developed in an aquifer-aquitard system.
2. The mixing processes in the reservoirs are important for solute transport in an aquifer-aquitard system.
3. The performance of the new analytical model is tested by the experimental data.

Abstract

Analytical models have been widely used to aid understanding the physical and chemical processes of tracer (or chemicals) in an aquifer-aquitard system in the laboratory-controlled experiment, when the observation data is few or not available during the experiment. When injecting tracer into (or extracting them from) the aquifer-aquitard system during experiments, the pre-inlet and after-outlet reservoirs are indispensable. However, the concentration variation in the reservoirs was not treated properly in previous analytical models, resulting in poor performance in interpreting experimental data. In this study, new mathematical models describing the concentration variation in the pre-inlet and the after-outlet reservoirs are proposed, and they are integrated into the novel analytical model. The novel analytical model is developed under the mobile-immobile (MIM) framework in the aquifer-aquitard system, considering the longitudinal and vertical dispersion, the advection, and the first-order chemical reaction in both aquifer and aquitard. A finite-difference solution is developed and the experimental data are employed to test the new analytical model. Results indicate that the concentration variation in the reservoirs is important to solute transport in the aquifer-aquitard system in the laboratory-controlled experiment, and the new analytical model outperforms the previous models in interpreting experimental data. The global sensitivity analysis demonstrates that the output concentration of solute transport in the aquifer-aquitard system is most sensitive to the volume of water in the pre-inlet reservoir. The contribution of the diffusion effect to the total mass flux of tracer crossing the aquifer-aquitard interface is much smaller than the contribution of the dispersive and advective effects.

Keywords: Solute transport; Vertical dispersion; Aquifer-aquitard system; Parameter estimation

1. Introduction

The laboratory-controlled experiment has been widely used to investigate solute transport in an aquifer-aquitard system. Due to the low permeability of fine sediments (such as clay and silt) consisting of aquitards, the groundwater release from aquitards is not easy to be observed or measured (Barbour et al., 2012; Rezanezhad et al., 2017; Rezanezhad et al., 2016; Xao et al., 2020). Alternatively, it is estimated by the mathematical models through interpreting the observed data in the adjacent aquifers (Li et al., 2021; Yang et al., 2016). Therefore, the robustness of the mathematical models is critical for understanding the mechanism of solute transport in an aquifer-aquitard system.

To date, many analytical models have been developed for solute transport in an aquifer-aquitard system. As the permeability of fine sediments of the aquitard is low, the flow velocity is much smaller than that in aquifer. In the early investigations of solute transport in the aquifer-aquitard system, the advective effect in the aquitard was ignored in the analytical models, such as Tang et al. (1981), Sudicky and Frind (1982), Sudicky et al. (1985), Starr et al. (1985), Chen (1985), Fujikawa and Fukui (1990), Roubinet et al. (2012), Zhou et al. (2017), Chen and Zhan (2018), Zhou and Zhan (2018), and Zhu and Zhan (2018). As the mechanical dispersion is dependent on velocity, ignoring advection implies that the dispersive effect is also ignored in the aquitard. In another word, only diffusion processes are considered in the aquitard in analytical models of the solute transport. Except Roubinet et al. (2012) and Chen and Zhan (2018), the other analytical models mentioned above assumed that the dispersion is one dimensional (1D) in the aquifer. Namely, the longitudinal dispersion is considered but the vertical dispersion is ignored in the aquifer, which means that tracer mixing processes finish instantaneously in the vertical profile of the aquifer. These models were named “averaged approximation” models

(Wang and Zhan, 2013; Zhan et al., 2009a). It was found that these models performed well in modeling solute transport in the fracture-matrix, as the fracture has much greater permeability and smaller aperture (Chen and Zhan, 2018; Zhou and Zhan, 2018; Zhou et al., 2017). The aquifer-aquitard system was different from the fracture-matrix system. This is because the aquifer permeability is smaller than the fracture permeability, and the vertical thickness is greater for the aquifer. As a result, the assumptions included in the "averaged approximation" models might be invalid for solute transport in the aquifer-aquitard system (Wang and Zhan, 2013). Then, the "averaged approximation" models have been extended by including the advective effect in the aquitard, such as Tang and Aral (1992); Zhan et al. (2009a); Zhan et al. (2009b); Liu et al. (2013); Rezaei et al. (2013); Wang and Zhan (2013); and Rezaei et al. (2016). Rezaei et al. (2016) considered two-dimensional (2D) dispersion and 1D advection in both aquifer and aquitard.

However, the currently published analytical models contain an assumption that the source concentration was treated as a constant (Liu et al., 2013; Rezaei et al., 2016) or a temporal-dependent variable which exponentially changes with time (Fujikawa and Fukui, 1990; Starr et al., 1985; Tang and Aral, 1992). Actually, such treatment could not be used to describe the variation of the source concentration in the laboratory-controlled experiments. Yang et al. (2016) and Li et al. (2021) conducted a two-dimensional (2D) laboratory-controlled experiment of solute transport, where the schematic diagram of the aquifer-aquitard system is as shown in Figure 1. There are two reservoirs connecting with aquifer, where the prepared tracer is injected pre-inlet reservoir. After mixing with original water in the pre-inlet reservoir, the tracer enters the aquifer-aquitard system. Therefore, the sources concentration is zero initially in the reservoir, and increases with time. Probably because the analytical model considering the variable source concentration in the pre-inlet reservoir is not available, Li et al. (2021) employed numerical

modeling to interpret the observation data of solute transport in the aquifer-aquitard system. Unfortunately, the mathematical model might be not robust, as the sources concentration variation was described by the temporal-dependent exponential function, which did not fully consider the mixing processes between the injected tracer and the original water in the pre-inlet reservoir. Meanwhile, the numerical errors (like numerical dispersion and numerical oscillations) are not be avoided completely in the numerical modeling when advection is dominant during solute transport (Yeh, 2000; Zheng and Wang, 1999).

Another assumption involved in the current analytical models is that the outlet boundary condition of the aquifer-aquitard system was not treated properly. There are two types of treatments. First, the aquifer horizontal extension was assumed to be infinite(Rezaei et al., 2016; Singh et al., 2020; Wang et al., 2020b). Such assumption performs well for the cases that the aquifer is long enough or the experimental time is short enough that tracer could not arrive in outlet boundary. Otherwise, after the tracer enters the after-outlet reservoir, as shown in Figure 1, such assumption could cause errors, which had been reported in the 1D column test (Wang et al., 2019). The second type of treatment is that the outlet boundary condition of solute transport was described by an exponential function with time in the analytical model (Tang and Aral, 1992). Such treatment is not based on physical processes of solute transport in the after-outlet reservoir.

Advection-dispersion equation (ADE) has been widely used to describe solute transport in subsurface (Baeumer et al., 2001; Chen et al., 2018; Van Genuchten, 1985; Zhan et al., 2009a). However, many recent studies demonstrated that the ADE model might not interpret the non-Fickian behaviors, like early breakthrough and long tails of breakthrough curves (BTCs) (Chen et al., 2017; Hansen et al., 2017; Wang et al., 2020b). Alternatively, the mobile-immobile (MIM) model was used instead of the ADE model. Zhou et al. (2017) derived a new analytical model of

solute transport using the MIM model. However, Zhou's model is based on the "averaged approximation", which might work well for solute transport in the fracture-matrix, but not in the aquifer-aquitard system.

In this study, the mathematical model of the concentration variation both in the pre-inlet and after-outlet reservoirs will be proposed based on the mass balance and Fick's law. Such models are integrated into the mathematical model of solute transport in the aquifer-aquitard system, which considers longitudinal and vertical dispersion, advection, and the first-order chemical reaction in both aquifer and aquitard. A novel analytical model is developed under the MIM framework. The numerical modeling and the experimental data reported by Li et al. (2021) are used to test the new analytical model. Global sensitivity analysis is conducted to investigate the influence of input parameters on the output concentration of solute transport.

2. Problem statement and mathematical model

The conceptual model of this study is composed of an aquifer and an overlain aquitard with uniform thickness, as shown in Figure 1. Both aquifer and aquitard are horizontal, homogeneous, and isotropic. The origin of the coordinate system is located at the left-lower corner of the aquifer. The x- and z- axes are horizontal and vertical, respectively.

Figure 1

2.1. 2D models of solute transport in an aquifer-aquitard system

Assuming that 1D advection, 2D dispersion, and the first-order chemical reaction are involved in the solute transport processes under the MIM framework, the governing equations of solute transport in the aquifer-aquitard system are

$$R_{\mathrm{m}}\frac{\partial C_{\mathrm{m}}}{\partial t}=D_x\frac{\partial^2 C_{\mathrm{m}}}{\partial x^2}+D_z\frac{\partial^2 C_{\mathrm{m}}}{\partial z^2}-v_x\frac{\partial C_{\mathrm{m}}}{\partial x}-\lambda_{\mathrm{m}}C_{\mathrm{m}}-\frac{\varepsilon}{\theta_{\mathrm{m}}}(C_{\mathrm{m}}-C_{\mathrm{im}}),\ 0\le z\le b_1,\ 0\le x\le L_{\mathrm{a}},\tag{1a}$$

$$R_{\mathrm{im}}\frac{\partial C_{\mathrm{im}}}{\partial t}=\frac{\varepsilon}{\theta_{\mathrm{im}}}(C_{\mathrm{m}}-C_{\mathrm{im}})-\lambda_{\mathrm{im}}C_{\mathrm{im}},\ 0\le z\le b_1,\ 0\le x\le L_{\mathrm{a}},\tag{1b}$$

$$R_{\mathrm{um}}\frac{\partial C_{\mathrm{um}}}{\partial t}=D_{\mathrm{uz}}\frac{\partial^2 C_{\mathrm{um}}}{\partial z^2}+D_{\mathrm{ux}}\frac{\partial^2 C_{\mathrm{um}}}{\partial x^2}-v_z\frac{\partial C_{\mathrm{um}}}{\partial z}-\lambda_{\mathrm{um}}C_{\mathrm{um}}-\frac{\varepsilon_{\mathrm{u}}}{\theta_{\mathrm{um}}}(C_{\mathrm{um}}-C_{\mathrm{uim}}),\ b_1\le z<b_1+b_2,\ 0\le x\le L_{\mathrm{a}},\tag{1c}$$

$$R_{\mathrm{uim}}\frac{\partial C_{\mathrm{uim}}}{\partial t}=\frac{\varepsilon_{\mathrm{u}}}{\theta_{\mathrm{uim}}}(C_{\mathrm{um}}-C_{\mathrm{uim}})-\lambda_{\mathrm{uim}}C_{\mathrm{uim}},\ b_1\le z<b_1+b_2,\ 0\le x\le L_{\mathrm{a}},\tag{1d}$$

where subscripts "m" and "im" are the parameters in the mobile and immobile domains, respectively; subscripts "u" is the parameters in the upper aquitard; x and z represent the vertical and horizontal distance [L], respectively; C_{m}, C_{im}, C_{um} and C_{uim} are the concentrations [ML^{-3}]; t is time [T]; b_1 and b_2 are the vertical thicknesses [L] of aquifer and aquitard, respectively; L_{a} is the horizontal length [L] of aquifer; v_x and v_z are the average velocities [LT^{-1}] of the aquifer and aquitard, respectively; $v_x=q_x/\theta_{\mathrm{m}}$, $v_z=q_z/\theta_{\mathrm{um}}$, q_x and q_z are the Darcy velocities [LT^{-1}] of the aquifer and aquitard, respectively; θ_{m}, θ_{im}, θ_{um} and θ_{uim} are the porosities [dimensionless]; λ_{m}, λ_{im}, λ_{um} and λ_{uim} are reaction rates [T^{-1}]; $R_{\mathrm{m}}=1+\frac{\rho_{\mathrm{b}}K_{\mathrm{d}}}{\theta_{\mathrm{m}}}$, $R_{\mathrm{im}}=1+\frac{\rho_{\mathrm{b}}K_{\mathrm{d}}}{\theta_{\mathrm{im}}}$, $R_{\mathrm{um}}=1+\frac{\rho_{\mathrm{b}}K_{\mathrm{d}}}{\theta_{\mathrm{um}}}$ and $R_{\mathrm{uim}}=1+\frac{\rho_{\mathrm{b}}K_{\mathrm{d}}}{\theta_{\mathrm{uim}}}$ are the retardation factors [dimensionless]; K_{d} is the equilibrium distribution coefficient [$M^{-1}L^3$]; ρ_{b} is the bulk density [ML^{-3}]; ε and ε_{u} are the first-order mass transfer coefficients [T^{-1}] of the aquifer and aquitard, respectively; D_x, D_z, D_{uz} and D_{ux} are the hydrodynamic dispersion coefficients [L^2T^{-1}], and one has

$$D_x=\alpha_x v_x+D_0,\tag{2a}$$

$$D_z=\alpha_z v_x+D_0,\tag{2b}$$

$$D_{\mathrm{uz}} = \alpha_{\mathrm{uz}} v_z + D_{\mathrm{u0}}, \tag{2c}$$

$$D_{\mathrm{ux}} = \alpha_{\mathrm{ux}} v_z + D_{\mathrm{u0}}, \tag{2d}$$

where α_x, α_z, α_{uz} and α_{ux} refer to dispersivities [L]; D_0 and D_{u0} are diffusion coefficients [L^2T^{-1}] of aquifer and aquitard, respectively.

The concentration and the flux at the aquifer-aquitard interface are assumed to be continuous, and one has

$$C_{\mathrm{m}}(x,z,t)|_{z=b_1} = C_{\mathrm{um}}(x,z,t)|_{z=b_1},\ 0 \le x \le L_{\mathrm{a}}, \tag{3a}$$

$$\left[\theta_{\mathrm{um}} v_z C_{\mathrm{um}}(x,z,t) - \theta_{\mathrm{um}} D_{\mathrm{uz}} \frac{\partial C_{\mathrm{um}}(x,z,t)}{\partial z}\right]\Big|_{z=b_1} = -\theta_{\mathrm{m}} D_z \frac{\partial C_{\mathrm{m}}(x,z,t)}{\partial z}\Big|_{z=b_1},\ 0 \le x \le L_{\mathrm{a}}, \tag{3b}$$

The lower and upper boundary conditions of solute transport in the aquifer-aquitard system are

$$\frac{\partial C_{\mathrm{m}}(x,z,t)}{\partial z}\Big|_{z=0} = 0,\ 0 \le x \le L_{\mathrm{a}}, \tag{4a}$$

$$C_{\mathrm{um}}(x,z,t)|_{z=b_1+b_2} = 0,\ 0 \le x \le L_{\mathrm{a}}, \tag{4b}$$

$$\left[v_x C_{\mathrm{m}}(x,z,t) - \alpha_x |v_x| \frac{\partial C_{\mathrm{m}}(x,z,t)}{\partial x}\right]\Big|_{x=0} = [v_x C_{\mathrm{in}}(t)]|_{x=0},\ 0 \le z \le b_1, \tag{4c}$$

$$\left[v_x C_{\mathrm{m}}(x,z,t) - \alpha_x |v_x| \frac{\partial C_{\mathrm{m}}(x,z,t)}{\partial x}\right]\Big|_{x=L_{\mathrm{a}}} = [v_x C_{\mathrm{out}}(t)]|_{x=L_{\mathrm{a}}},\ 0 \le z \le b_1, \tag{4d}$$

where $C_{\mathrm{in}}(t)$ and $C_{\mathrm{out}}(t)$ are the concentrations [ML^{-3}] in the pre-inlet and after-outlet reservoirs, respectively. They could be computed by the models in Section 2.2.

The initial conditions used in this study are

$$C_{\mathrm{m}}(x,z,t)|_{t=0} = C_{\mathrm{im}}(x,z,t)|_{t=0} = C_{\mathrm{um}}(x,z,t)|_{t=0} = C_{\mathrm{uim}}(x,z,t)|_{t=0} = 0,\ 0 \le z < b_1 + b_2,\ 0 \le x \le L_{\mathrm{a}}. \tag{5}$$

The new model is an extension of some previous models. For instance, when $C_{\mathrm{in}}(t) = 1$, $D_{\mathrm{ux}} = 0$, $L_{\mathrm{a}} \to \infty$, and $\varepsilon = \varepsilon_{\mathrm{u}}$, the new model reduces to the model of Zhan et al. (2009a). If $C_{\mathrm{in}}(t) = 1$, $D_z = D_{\mathrm{ux}} = 0$, $v_z = 0$, and $L_{\mathrm{a}} \to \infty$, the new model becomes the model of Zhou et

al. (2017). When $\varepsilon = \varepsilon_{\mathrm{u}},\ C_{\mathrm{in}}(t) = C_1(z)exp(-\zeta_1 t),\ C_{\mathrm{out}}(t) = C_2(z)exp(-\zeta_2 t)$, in which $C_1(z)$ and $C_2(z)$ are the concentrations [ML^{-3}] in the inner and outer boundary conditions, respectively; ζ_1 and ζ_2 are constants [T^{-1}], the new model reduces to the solution of Tang and Aral (1992). If $C_{\mathrm{in}}(t) = 1,\ D_x = D_z = D_{\mathrm{ux}} = 0,\ v_z = 0,\ L_{\mathrm{a}} \to \infty,\ \varepsilon = \varepsilon_{\mathrm{u}},\ \lambda_{\mathrm{m}} = \lambda_{\mathrm{um}} = 0,$ the new model becomes to the model of Zhu and Zhan (2018).

2.2 Models describing concentration variation in reservoirs

Assuming the injected tracer instantaneously and completely mixes with the original water in the pre-inlet reservoir, the concentration variation in the pre-inlet reservoir could be described as following equations based on the mass balance and the Fick's law

$$V_{\mathrm{in}} \frac{dC_{\mathrm{in}}(t)}{dt} = -Q_{\mathrm{in}}[C_{\mathrm{in}}(t) - C_0]|_{x=0},\ 0 \le z \le b_1, \tag{6a}$$

$$C_{\mathrm{in}}(t)|_{t=0} = 0,\ 0 \le z \le b_1, \tag{6b}$$

where V_{in} is the volume [L^3] of water in the pre-inlet reservoir; $V_{\mathrm{in}} = L_{\mathrm{in}} w_{\mathrm{in}} h_{\mathrm{in}}$; L_{in} and w_{in} are the length and width [L] of the pre-inlet reservoir, respectively; h_{in} is the water level in the pre-inlet reservoir; Q_{in} represents the flow rate [L^3T^{-1}] entering the aquifer; $Q_{\mathrm{in}} = b_1 w_{\mathrm{in}} \theta_{\mathrm{m}} v_x$; C_0 is concentration [ML^{-3}] of the prepared tracer, which is a constant. The first and second terms on the right side of Eq. (6a) represent the mass of tracer injected into the reservoir, and the mass of tracer after mixing with water term leaving the reservoir.

Similarly, the mathematical model describing the concentration variation in the after-outlet reservoir could be obtained

$$V_{\mathrm{out}} \frac{dC_{\mathrm{out}}(t)}{dt} = w_{\mathrm{out}} b_1 D_x \frac{dC_{\mathrm{m}}(x,z,t)}{dx}\Big|_{x=L_{\mathrm{a}}},\ 0 \le z \le b_1, \tag{7a}$$

$$C_{\mathrm{out}}(t)|_{t=0} = 0,\ 0 \le z \le b_1, \tag{7b}$$

where V_{out} is the volume [L^3] of water in the after-outlet reservoir; $V_{\mathrm{out}} = L_{\mathrm{out}} w_{\mathrm{out}} h_{\mathrm{out}}$; L_{out} and w_{out} are the length and width [L] of the after-outlet reservoir, respectively; h_{out} is the water level in the after-outlet reservoir.

By checking the models of Eqs. (6) - (7), one may find that if the concentration variation in the reservoirs is not measured during the experiment or the observation data is not available, $C_{\mathrm{in}}(t)$ and $C_{\mathrm{out}}(t)$ could be computed using the parameters of injection rate, water volume of the reservoirs, and the concentration of the injected tracer.

3. Solutions of 2D solute transport in an aquifer-aquitard system

3.1. Analytical solutions in Laplace domain

Eqs. (1) - (7) composed the mathematical model describing the 2D solute transport in an aquifer-aquitard system. In this study, the Laplace transform method and the finite-cosine Fourier transform method will be employed to derive the analytical model in Laplace domain. The detailed derivations could be seen in ***Appendix A***.

In the aquifer, the solutions in the Laplace domain are

$$\bar{C}_{\mathrm{m}} = \sum_{\mathrm{n}=0}^{\infty} [\mathrm{N_n} exp(\alpha_{\mathrm{n}} x) + \mathrm{D_n} exp(\delta_{\mathrm{n}} x)] cos(\omega_{\mathrm{n}} z),\ 0 \le z \le b_1,\ 0 \le x \le L_{\mathrm{a}}, \tag{8a}$$

$$\bar{C}_{\mathrm{im}} = \frac{\varepsilon/\theta_{\mathrm{im}}}{\varepsilon/\theta_{\mathrm{im}} + \lambda_{\mathrm{im}} + R_{\mathrm{im}} s} \bar{C}_{\mathrm{m}},\ 0 \le z \le b_1,\ 0 \le x \le L_{\mathrm{a}}, \tag{8b}$$

where the over bar refers to the terms in Laplace domain hereinafter; s denotes the Laplace transform parameter in respect to t; ω_{n} is the frequency terms used in the Fourier transform and it could be computed by Eq. (10); n is a positive integer;

$$\mathrm{N_n} = \frac{g(s) \frac{4 sin(b_1 \omega_{\mathrm{n}})}{2 b_1 \omega_{\mathrm{n}} + sin(2 b_1 \omega_{\mathrm{n}})}}{(1 - \alpha_{\mathrm{n}}) - \frac{(1 - \delta_{\mathrm{n}})(\alpha_{\mathrm{n}} - \delta s) exp(\alpha_{\mathrm{n}} L_{\mathrm{a}} - \delta_{\mathrm{n}} L_{\mathrm{a}})}{\delta_{\mathrm{n}} - \delta s}} \mathrm{D_n};\ \mathrm{D_n} = -\frac{(\alpha_{\mathrm{n}} - \delta s) exp(\alpha_{\mathrm{n}} L_{\mathrm{a}} - \delta_{\mathrm{n}} L_{\mathrm{a}})}{\delta_{\mathrm{n}} - \delta s} \mathrm{N_n};$$

241 $g(s) = \frac{C_0}{s(sV_{\text{in}}/Q_{\text{in}}+1)}$; $\delta = \frac{V_{\text{out}}}{w_{\text{out}}h_{\text{out}}D_x}$; $\alpha_{\text{n}} = \frac{v_x - \sqrt{v_x^2+4D_x(E_1+\omega_{\text{n}}^2)}}{2D_x}$; $\delta_{\text{n}} = \frac{v_x + \sqrt{v_x^2+4D_x(E_1+D_z\omega_{\text{n}}^2)}}{2D_x}$;

242 $E_1 = \lambda_{\text{m}} + R_{\text{m}}s + \varepsilon/\theta_{\text{m}} - \frac{\varepsilon^2/\theta_{\text{m}}\theta_{\text{im}}}{\varepsilon/\theta_{\text{im}}+\lambda_{\text{im}}+R_{\text{im}}s}$.

243 In the aquitard, the analytical solutions in Laplace domain are

244 $\bar{C}_{\text{um}} = \sum_{\text{n}=0}^{\infty}[\text{A}_{\text{n}}exp(\beta_{\text{n}}z) + \text{B}_{\text{n}}exp(\sigma_{\text{n}}z)] \times [\text{N}_{\text{n}}exp(\alpha_{\text{n}}x) + \text{D}_{\text{n}}exp(\delta_{\text{n}}x)]$, $b_1 \le z <$

245 $b_1 + b_2, 0 \le x \le L_{\text{a}}$, (9a)

246 $\bar{C}_{\text{uim}} = \frac{\varepsilon_{\text{u}}/\theta_{\text{uim}}}{\varepsilon_{\text{u}}/\theta_{\text{uim}}+\lambda_{\text{uim}}+R_{\text{uim}}s}\bar{C}_{\text{um}}, b_1 \le z < b_1 + b_2, 0 \le x \le L_{\text{a}}$, (9b)

247 where $\text{A}_{\text{n}} = -\frac{cos(\omega_{\text{n}}b_1)exp[\sigma_{\text{n}}(b_1+b_2)-\beta_{\text{n}}(b_1+b_2)]}{exp[\sigma_{\text{n}}b_1]-exp[\sigma_{\text{n}}(b_1+b_2)-\beta_{\text{n}}b_2]}$; $\text{B}_{\text{n}} = \frac{cos(\omega_{\text{n}}b_1)}{exp[\sigma_{\text{n}}b_1]-exp[\sigma_{\text{n}}(b_1+b_2)-\beta_{\text{n}}b_2]}$; $E_2 =$

248 $\lambda_{\text{um}} + sR_{\text{um}} + \varepsilon_{\text{u}}/\theta_{\text{uim}} - \frac{\varepsilon_{\text{u}}^2/\theta_{\text{um}}\theta_{\text{uim}}}{\varepsilon_{\text{u}}\theta_{\text{uim}}+\lambda_{\text{uim}}+R_{\text{uim}}s}$; $\beta_{\text{n}} = \frac{v_z - \sqrt{v_z^2+4D_{\text{uz}}(E_2+D_{\text{ux}}\alpha_{\text{n}}^2)}}{2D_{\text{uz}}}$;

249 $\sigma_{\text{n}} = \frac{v_z + \sqrt{v_z^2+4D_{\text{uz}}(E_2+D_{\text{ux}}\alpha_{\text{n}}^2)}}{2D_{\text{uz}}}$.

250 The values of ω_n are the positive solution of the following function

251 $\omega_{\text{n}}tan(\omega_{\text{n}}b_1) = \frac{W_1[v_z exp(\beta_{\text{n}}b_1) - D_{\text{uz}}\beta_{\text{n}}exp(\beta_{\text{n}}b_1)]}{D_z} + \frac{W_2[v_z exp(\sigma_{\text{n}}b_1) + D_{\text{uz}}\sigma_{\text{n}}exp(\sigma_{\text{n}}b_1)]}{D_z}$, (10)

252 where $W_1 = -\frac{\theta_{\text{um}}}{\theta_{\text{m}}}\frac{exp[\sigma_{\text{n}}(b_1+b_2)-\beta_{\text{n}}(b_1+b_2)]}{exp[\sigma_{\text{n}}b_1]-exp[\sigma_{\text{n}}(b_1+b_2)-\beta_{\text{n}}b_2]}$ and $W_2 = \frac{\theta_{\text{um}}/\theta_{\text{m}}}{exp[\sigma_{\text{n}}b_1]-exp[\sigma_{\text{n}}(b_1+b_2)-\beta_{\text{n}}b_2]}$.

253 ***3.2. Solutions in real-time domain***

254 Eqs. (8) - (9) are analytical solutions of solute transport in the aquifer-aquitard system in

255 Laplace domain. As the mathematical expression of ω_{n} included in these equations is complex,

256 the analytical solutions could not be derived easily in the real-time domain from the Laplace

257 domain. Alternatively, the numerical inverse Laplace transform method will be adopted to do so.

258 There are several numerical inverse Laplace transform methods available, such as the Stehfest

259 method (Stehfest and Harald, 1970a; Stehfest and Harald, 1970b), the Schapery method

(Schapery, 1962), the Fourier series method (Dubner and Abate, 1968), and so on. The Stehfest method was demonstrated to perform well in solving the problems related to solute transport (Wang et al., 2020a; Wang et al., 2020b), and will be employed to conduct the inverse Laplace transform on Eqs. (8) - (9) in this study.

4. Comparison of the new analytical model with numerical modeling

In this study, the new analytical model is derived by the Laplace transform method and the finite-cosine Fourier transform method. However, the solutions are in Laplace domain, and it needs to conduct numerical inverse Laplace transform to obtain the real-time domain solutions. To test the new analytical model of this study, a high-resolution finite-difference solution will be employed. The details for discretization could be seen in ***Appendix B.*** Eqs. (B5a) - (B5d) are ordinary differential equations, and they could be solved by stiff integrator ODE 15s in MATLAB (Shampine and Reichelt, 1997).

Figures 2a and 2b show the comparison between numerical modeling and analytical model. The parameters used in this case are: $v_x = 0.5486\text{m} \cdot \text{h}^{-1}$; $v_z = 0.0069\text{m} \cdot \text{h}^{-1}$; $\alpha_x = 0.5\text{m}$; $\alpha_z = \alpha_{\text{uz}} = \alpha_{\text{ux}} = 0.1\text{m}$; $D_0 = D_{\text{u0}} = 10^{-7}\text{m}^2 \cdot \text{h}^{-1}$; $R_{\text{m}} = R_{\text{im}} = R_{\text{um}} = R_{\text{uim}} = 1$; $\theta_{\text{m}} = 0.37$; $\theta_{\text{im}} = 0.01$; $\theta_{\text{um}} = 0.52$; $\theta_{\text{uim}} = 0.01$; $\varepsilon = \varepsilon_{\text{u}} = 0.0001\text{h}^{-1}$; $\lambda_{\text{m}} = \lambda_{\text{im}} = \lambda_{\text{um}} = \lambda_{\text{uim}} = 10^{-6}\text{h}^{-1}$; $Q_{\text{in}} = 0.0049\text{m}^3 \cdot \text{h}^{-1}$; $b_1 = 0.24\text{m}$; $b_2 = 0.29\text{m}$; $w_{\text{in}} = w_{\text{out}} = 0.1\text{m}$; $h_{\text{in}} = h_{\text{out}} = 0.745\text{m}$; $L_{in} = L_{out} = 0.10\text{m}$; $L_a = 0.70\text{m}$; $V_{\text{in}} = V_{\text{out}} = 0.00745\text{m}^3$. The values of these parameters are from the experiment of Li et al. (2021). Figures 2a and 2b indicate that the analytical model agrees very well with the numerical solution, demonstrating that the Stehfest method performs well in conducting the inverse Laplace transform on Eqs. (8) - (9) of this study.

Figure 2

5. Applications

To test the performance of new model, the observation data of solute transport in a 2D experiment by Li et al. (2021) will be employed. In the aquifer-aquitard system, the aquifer dimension is 0.70m in length, 0.10m in width and 0.24m in thickness, and the aquitard dimension is 0.70m in length, 0.10m in width and 0.29m in thickness. The experimental setup is as shown in Figure 1 of Li et al. (2021). The dimensions of the pre-inlet and after-outlet reservoirs are the same and 0.10m in length, 0.10m in width and 0.745m in thickness. The lithologies of the aquifer and aquitard are coarse sand with grain sizes ranging from 0.50 to 0.90mm and well sorted clay, respectively. The hydraulic conductivities of aquifer and aquitard are$1.459\mathrm{m}\cdot\mathrm{h}^{-1}$ and $0.000129\mathrm{m}\cdot\mathrm{h}^{-1}$, respectively. The porosities of aquifer and aquitard are 0.37 and 0.52, respectively. The hydraulic heads are 1.486m and 1.437m in pre-inlet and after-outlet reservoirs, respectively. They keep constant during the entire experiment. After the flow flied is in the steady state, the tracer is injected into the pre-inlet reservoir. As the top elevation of the aquitard (e.g., 0.53m) is smaller than the hydraulic heads in the reservoirs, the aquifer is confined under the steady-state flow field. Li et al. (2021) employed the Darcy's law to compute the 1D averaged Darcy velocities, and they were $q_x = 0.203\mathrm{m}\cdot\mathrm{h}^{-1}$ and $q_z = 0.000359\mathrm{m}\cdot\mathrm{h}^{-1}$, respectively.

To interpret the experimental data of solute transport in the aquifer-aquitard system, Li et al. (2021) employed a 2D ADE model as the governing equation, where the hydrodynamic dispersion and advection are 2D in both aquifer and aquitard. As for the source concentration in the pre-inlet reservoir, they employed an exponential function to describe the variation

$$C_{\mathrm{in}}(t) = C_0[1 - \exp(-\zeta t)], \tag{11}$$

where ζ is a constant [T^{-1}]. Since the observation data of the concentration in the pre-inlet reservoir ($C_{\mathrm{in}}(t)$) is not available in the experiment of Li et al. (2021) (probably not measured), the values of ζ could not be estimated directly. By checking the fitness of observed BTCs by the 2D ADE model (Figures 7 and 8 in Li et al. (2021) or Figures 3 and 4 in this study), one may find that it is not very well, especially at the observation points of (55), (13), (33), (14), (15) and (25). The spatial locations of observation points could be seen in Figure 1 of Li et al. (2021). In this study, the 2D ADE model used in Li et al. (2021) is called Li's model. As the lithologies of the aquifer and aquitard are almost homogeneous, we may assume that the 2D ADE model could be used to describe the solute transport in the aquifer-aquitard system. Therefore, such large errors caused by Li's model might originate from the two types of issues. Firstly, Eq. (11) might not accurately describe the source concentration variation in the pre-inlet reservoir. Secondly, the parameters used in the 2D ADE model could not represent the real processes of solute transport.

Figure 3

To test the performance of the analytical model of this study, we employ Eqs. (8) - (9) to reinterpret the observation data. The first type of issue resulting in errors by Li's model could be solved using the model of this study. As mentioned in Section 2.2, the values of $C_{\mathrm{in}}(t)$ could be computed if the parameters of injection rate, water volume of the reservoirs, and C_0 are given. These parameters could be found in Li et al. (2021): $Q_{\mathrm{in}} = 0.0049\mathrm{m}^3 \cdot \mathrm{h}^{-1}$, and $V_{\mathrm{in}} = V_{\mathrm{out}} = 0.00745\mathrm{m}^3$. C_0 is included in the relative concentration (C/C_0), as shown in Figures 3 and 4. As for the first type of issue, we estimate the parameters using the trial-and-error method, and they are: $v_z = 0.0001\mathrm{m} \cdot \mathrm{h}^{-1}$; $\alpha_x = 0.025\mathrm{m}$; $\alpha_z = 0.015\mathrm{m}$; $\alpha_{\mathrm{uz}} = \alpha_{\mathrm{ux}} = 0.02\mathrm{m}$. The other parameters involved in the analytical model are measured in the experiment, and the values are same as ones used in Figure 2. The fitness of observed BTCs by the new analytical model is

shown in Figures 3 and 4. For the sake of comparison, the computed BTCs by Li's model are also included. Results show that the analytical model of this study performs better than Li's model. Table 1 shows the errors between observed and computed BTCs, where the errors are computed by (Moriasi et al., 2007)

$$\mathrm{RSR} = \frac{\sqrt{\sum_{i=1}^{\mathrm{NN}}\left(Y_i^{obs} - Y_i^{est}\right)^2}}{\sqrt{\sum_{i=1}^{\mathrm{NN}}\left(Y_i^{obs} - Y^{mean}\right)^2}}, \tag{12}$$

where Y_i^{obs} is the i^{th} observed value, Y_i^{est} is the i^{th} estimated value, Y^{mean} is the mean of the observation data, and NN is the total number of observations. A smaller RSR means that the model is more accurate. The model is perfect when $\mathrm{RSR} = 0$. Obviously, the values of RSR are smaller for the model used in this study than Li's model.

Figure 4

Table 1

As the advection is 2D in the governing of Li et al. (2021), but it is 1D in this study, Li's model is an extension of the analytical model of this study when $\varepsilon = 0$. The parameters estimated in this study are different from ones used in Li's model, which are $v_z = 0.0069\mathrm{m} \cdot \mathrm{h}^{-1}$; $\alpha_x = 0.0045\mathrm{m}$; $\alpha_z = 0.004\mathrm{m}$; $\alpha_{\mathrm{uz}} = \alpha_{\mathrm{ux}} = 0$. Probably, one may raise two questions about the performance of the new analytical model. Firstly, in the analytical model of this study, the flow velocity is assumed to be horizontal in the aquifer and vertical in the aquitard. Although such an assumption has been widely used in the analytical models to approximate the 2D velocity, it may cause great errors in interpreting the experimental data. To answer this question, we compare the solutions by Li's model and the analytical model of this study under the special case, where $\varepsilon = 0$ and Eq. (11) are used to describe the source concentration instead of Eqs. (6a) - (6b) in the analytical model. "$\varepsilon = 0$" means that the MIM model reduces to the ADE model.

The other parameters used in these two models are the same. The results are as shown in Figures 5a and 5b, the difference between them is not obvious exception when $t < 0.5$h. Therefore, one may conclude that the assumption related the advection used in the analytical model is robust.

The second question is that the larger errors caused by Li's model might be due to the second type of issue mentioned above, not the first type of issue. In another word, the errors caused by Eq. (11) might be negligible, and the fitness of observed BTCs by Li's model could be improved by adjusting the parameter values. To test whether Eq. (11) could be used to describe the source concentration properly, we compare the models by Li's model and the analytical model of this study when $\varepsilon = 0$. The source concentration is described by Eqs. (6a) - (6b) in the analytical model of this study, and by Eq. (11) in Li's model. The parameters used in these two models are the same, except $\zeta = 0.000575\text{h}^{-1}$ used in Li's model and $C_{\text{in}}(t)$ computed by Eqs. (6a) - (6b). Figures 5a and 5b show the differences between two models are obvious. Therefore, the errors caused by Eq. (11) are not negligible, and the performance of the new analytical model is better.

Figure 5

6. Results and Discussions

6.1. Effect of V_{in} on solute transport in aquifer-aquitard system

In this study, new models describing the concentration variation in the reservoirs connecting aquifer-aquitard system are proposed and incorporated in the analytical model of solute transport in the aquifer-aquitard system. From Eq. (6), one may find that V_{in} is a main parameter influencing $C_{\text{in}}(t)$. To test the effect of V_{in} on solute transport in aquifer-aquitard system, three sets of V_{in} are employed: $V_{\text{in}} = 0$, 0.005m^3 and 0.01m^3. The other parameters are the same as

ones used in Figure 2. Figures 6 and 7 show the comparison of BTCs and the residence time distributions (RTDs) for different V_{in} and z, respectively.

Two interesting observations could be found in Figure 6. Firstly, BTCs decrease with increasing V_{in}. When $V_{\mathrm{in}} = 0$, BTC is largest. "$V_{\mathrm{in}} = 0$" implies that the tracer concentration in pre-inlet reservoir is the same as the concentration of the injected tracer during the entire experiment, which is not true but for the purpose of comparison. Such observation could be explained as follows. A larger V_{in} means that there is a larger volume original water in the pre-inlet reservoir. After the injected tracer mixes with the original water in the reservoir, the tracer concentration becomes smaller. Therefore, a larger V_{in} makes a smaller tracer concentration in the reservoir. The case of $V_{\mathrm{in}} = 0$ means the volume of water the reservoir is zero, and no mixing processes occur between the injected tracer and original water in the pre-inlet reservoir. Secondly, the influence of V_{in} on BTCs is larger in the aquifer than that in the aquitard. This is because the aquifer has larger permeability resulting in the greater advection and dispersion, and the tracer moves faster in the aquifer.

Figure 6

Figure 7 shows the influence of V_{in} on RTDs. RTD is a unimodal and asymmetric curve. One may find that such influence is obvious, and a larger V_{in} makes RTD flatter. The peak values of RTDs decrease with increasing V_{in}, while the time corresponding to the peak value increases with increasing V_{in}.

Figure 7

6.2. Mass flux crossing the aquifer-aquitard interface

As the aquitard has low permeability, the flow velocity is generally small. Then, many previous studies ignored the effects of dispersion and advection during solute transport in the

aquitard (Sudicky and Frind, 1982; Sudicky et al., 1985; Tang et al., 1981). As a result, the mass flux (MF) crossing the aquifer-aquitard interface is underestimated. However, numerous recent studies demonstrated that MF of the chemicals from the aquitard might be an important factor influencing the water quality in the adjacent aquifer, since the clayey aquitard is enriched in heavy metal elements (Guerrero et al., 1993; Hendry et al., 2004; Lin and Puls, 2000; Mazurek et al., 2011).

MF is an important variable to show how much tracer enters or releases from the aquitard, and it is affected by the diffusion, dispersion, and advection. Figure 8 shows the variation of MF with distance at different times. MF is computed by Eq. (3). The parameters used in this figure are same as ones used in Figure 3. Two interesting observations could be found. Firstly, MF decreases with distance along the x axis. This is because the origin of the coordinate system is located at the inlet boundary, where the concentration is maximum. Secondly, MF increases with the time. This observation could be explained by the boundary conditions of the aquifer-aquitard interface. As the diffusion, dispersion, and flow velocity are constant in the aquitard, MF is controlled by the concentration at the aquifer-aquitard interface, which increases with time.

Figure 8

Figure 9 shows the contributions of the diffusion, dispersion, and advection in aquitard on MF. The legend of MF_{ADD} means total mass flux of tracer crossing the aquifer-aquitard interface, which is calculated by considering diffusion, dispersion, and advection. The legend of MF_{Adv}, MF_{Dis} and MF_{Dif} respectively represent the calculation of MF only considering advection, MF only considering dispersion, and MF only considering diffusion. One may find that the contributions of these three processes from large to small is advection, dispersion, and diffusion. The ratio of MF_{Dif} to MF_{ADD} is 0.01% which is almost zero, implying that the effect of diffusion

on MF might be negligible in the short time of interest. The contributions of MF_{Adv} and MF_{Dis} to MF_{ADD} are about 11% and 89%, respectively. Therefore, the models ignoring the advection and dispersion could greatly underestimate MF crossing the aquifer-aquitard interface.

Figure 9

6.3. Global sensitivity analysis

From the analytical model of Eqs. (8) - (9), one may find that the main parameters affecting BTCs are: v_x, v_z, α_x, α_z, α_{uz}, α_{ux}, θ_{u}, θ_{m}, b_1, b_2, R_{um}, R_{m}, ε, ε_{u}, λ, λ_{u}, V_{in} and V_{out}. To test how these parameters affect the solute transport in the aquifer-aquitard system, the global sensitivity analysis is conducted. To date, there are many global sensitivity analysis methods available, such as the Morris screening method (Morris, 1991), regression analysis (Tiscareno-Lopez et al., 1993), variance-based method (Saltelli et al., 2008), meta-modeling method (Sathyanarayanamurthy and Chinnam, 2009), and so on. As the Morris screening method has lower computation, it will be used in this study (Morris, 1991)

$$\sigma_i = \sqrt{\frac{1}{j}\sum_{l=1}^{j}\left(E_i^l - \mu_i\right)^2}, i = 1,2,\dots,I, \tag{13a}$$

$$\mu_i^* = \sum_{l=1}^{j}\left(\left|E_i^l\right|/j\right), i = 1,2,\dots,I, \tag{13b}$$

$$\mu_i = \sum_{l=1}^{j}\left(E_i^l/j\right), i = 1,2,\dots,I, \tag{13c}$$

where σ_i and μ_i^* are the standard deviation and absolute mean of sample points, respectively; a larger μ_i^* means greater sensitivity of the i^{th} parameter on the output results, while the larger σ_i implies higher interaction effects and/or non-linear effects of the i^{th} parameter than others; j is the total number of the sample points and $j = 30$ in this study; I is the number of the total number of parameters and $I = 18$ in this study; $E_i^l = \frac{C_{\mathrm{m}}(p_1,p_2,\dots,p_i+l\Delta,\dots,p_n) - C_{\mathrm{m}}(p_1,p_2,\dots,p_i,\dots,p_n)}{l\Delta}$; where p_i is a value of the i^{th} input parameter in the range of $\left(p_{i,0}, p_{i,lim}\right)$; $p_{i,0}$ and $p_{i,lim}$ are

the smallest and the largest values of p_i, respectively, as shown in Table 2; Δ represents a small increment and $\Delta = 1/(j-1)$.

Figures 10a and 10b show that the variation of μ_i^* and σ_i with time in the aquifer (at $z = 0.16\text{m}$ and $x = 0.10\text{m}$), respectively. Figure 10a indicates that the values of μ_i^* from large to small is V_{in}, θ_{m}, v_x, α_x, α_{uz}, α_{z}, θ_{u}, α_{ux}, v_z, b_1, R_{m}, ε, ε_{u}, V_{out}, b_2, R_{um}, λ_{m} and λ_{um}. It implies the concentration is more sensitive to the change in V_{in}, θ_{m} and v_z than the other parameters. Figure 10b shows that the order of σ_i from large to small is V_{in}, θ_{m}, v_x, α_x, α_{ux}, α_{ux}, θ_{u}, α_z, v_z, b_1, R_{m}, b_2, ε_{u}, ε, R_{um}, λ_{m}, λ_{um} and V_{out}. It means that V_{in}, θ_{m} and v_x have the higher interaction effects and/or non-linear effects than others.

In summary, the output concentration of solute transport in the aquifer-aquitard system is most sensitive to V_{in}, demonstrating that the variation of the tracer concentration in the pre-inlet reservoir is important for solute transport in an aquifer-aquitard system in the laboratory-controlled experiment.

Figure 10

Table 2

7. Summary and conclusions

The laboratory-controlled experiment is an effective technique to investigate the mechanism of solute transport in an aquifer-aquitard system. When injecting tracer (or chemicals) into (or extracting them from) the aquifer or aquitard during experiments, reservoirs are indispensable. As the observation data is generally few during the experiment, mathematical modeling has been widely used to aid understanding the physical and chemical processes of tracer. However, the concentration variation in the reservoirs did not be treated properly in previous analytical models, resulting in poor performance in interpreting experimental data. In this study, we develop the

new mathematical models describing the concentration variation in pre-inlet and after-outlet reservoirs. Such models are incorporated into the mathematical model of solute transport in the aquifer-aquitard system, and a novel analytical model is derived by Laplace transform method and the finite-cosine Fourier transform method under the MIM framework. The new analytical model considers the longitudinal and vertical dispersion, the advection, and the first-order chemical reaction in both aquifer and aquitard. The new analytical model is tested by the finite-difference solution and the experimental data reported by Li et al. (2021). The global sensitivity analysis method of Morris (1991) is conducted to investigate the influences of input parameters on the output concentration of solute transport. The following conclusions could be drawn from this study.

(1) When the concentration variation in the reservoirs is not measured during the experiment or the observation data is not available, it could be computed using the parameters of injection rate, water volume of the reservoirs, and the concentration of the injected tracer by the new models of this study.

(2) The new analytical model outperforms the previous models in interpreting experimental data.

(3) The influence of V_{in} on BTCs and RTDs is obvious and not negligible. BTCs decreases with increasing V_{in}. The peak values of RTDs decrease with increasing V_{in}, while the time corresponding to the peak value increases with increasing V_{in}.

(4) The effect of diffusion on total mass flux of tracer (MF_{ADD}) is about 0.1%, and could be negligible in the short time of interest, while the contributions of MF_{Adv} and MF_{Dis} to MF_{ADD} are about 11% and 89%, respectively.

(5) The global sensitivity analysis shows the variation of the tracer concentration in the pre-inlet reservoir is important for solute transport in an aquifer-aquitard system in the laboratory-controlled experiment.

Acknowledgments

- This research was partially supported by Programs of Natural Science Foundation of China (No.41772252, No. 41972250 and No.41502229); Innovative Research Groups of the National Nature Science Foundation of China (No. 41521001), the Fundamental Research Funds for the Central Universities, and China University of Geosciences (Wuhan) (No. CUGGC07); the 111 Program (State Administration of Foreign Experts Affairs & the Ministry of Education of China, No. B18049).

Declaration of interests

- The authors declare that they have no known competing financial interests or personal relationships that could have appeared to influence the work reported in this paper.

Appendix A. Derivation of analytical solution

Conducting Laplace transform to Eqs. (1a) - (1b) and Eqs. (6) - (7), one has

$$D_x \frac{\partial^2 \bar{C}_\mathrm{m}}{\partial x^2} + D_z \frac{\partial^2 \bar{C}_\mathrm{m}}{\partial z^2} - v_x \frac{\partial \bar{C}_\mathrm{m}}{\partial x} - E_1 \bar{C}_\mathrm{m} = 0 = 0,\ 0 \le z \le b_1,\ 0 \le x \le L_\mathrm{a}, \tag{A1}$$

$$\bar{C}_\mathrm{im} = \frac{\varepsilon/\theta_\mathrm{im}}{\varepsilon/\theta_\mathrm{im}+\lambda_\mathrm{im}+R_\mathrm{im}s} \bar{C}_\mathrm{m},\ 0 \le z \le b_1,\ 0 \le x \le L_\mathrm{a}, \tag{A2}$$

$$\left[\bar{C}_\mathrm{m}(x,z,s) - \alpha_x \frac{\partial \bar{C}_\mathrm{m}(x,z,s)}{\partial x}\right]\Big|_{x=0} = g(s),\ 0 \le z \le b_1, \tag{A3}$$

$$\frac{d\bar{C}_\mathrm{m}(x,z,s)}{dx}\Big|_{x=L_a} = \delta s \bar{C}_\mathrm{out}(x,z,s)|_{x=L_a},\ 0 \le z \le b_1, \tag{A4}$$

where $E_1 = \lambda_\mathrm{m} + R_\mathrm{m}s + \varepsilon/\theta_\mathrm{m} - \frac{\varepsilon^2/\theta_\mathrm{m}\theta_\mathrm{im}}{\varepsilon/\theta_\mathrm{im}+\lambda_\mathrm{im}+R_\mathrm{im}s}$; $g(s) = \frac{1}{s(sV_\mathrm{in}/Q_\mathrm{in}+1)}$; $\delta = \frac{V_\mathrm{out}}{w_\mathrm{out}h_\mathrm{out}D_x}$.

Assuming the solution of Eq. (A1) is

$$F = \sum_{n=0}^{\infty} \bar{C}_m cos(\omega_n z), \quad \text{(A5)}$$

Substituting Eq. (A5) into Eq. (A1), one has

$$D_x \frac{\partial^2 F}{\partial x^2} - v_x \frac{\partial F}{\partial x} - (E_1 + D_z \omega_n^2) F = 0, \quad \text{(A6)}$$

where ω_n is the frequency terms used in the Fourier transform.

Eq. (A6) is an ordinary differential equation, and the general solution is

$$F = N_n exp(\alpha_n x) + D_n exp(\delta_n x), \quad \text{(A7)}$$

where $\alpha_n = \frac{v_x - \sqrt{v_x^2 + 4D_x(E_1 + D_z\omega_n^2)}}{2D_x}$ and $\delta_n = \frac{v_x + \sqrt{v_x^2 + 4D_x(E_1 + D_z\omega_n^2)}}{2D_x}$.

Thus, the solution of Eq. (A1) is

$$\bar{C}_m = \sum_{n=0}^{\infty} [N_n exp(\alpha_n x) + D_n exp(\delta_n x)] cos(\omega_n z), \quad \text{(A8)}$$

According to the boundary conditions of Eqs. (A3) - (A4), the coefficients of N_n and D_n could be obtained, yields $N_n = \frac{g(s)\frac{4sin(b_1\omega_n)}{2b_1\omega_n + sin(2b_1\omega_n)}}{(1-\alpha_n) - \frac{(1-\delta_n)(\alpha_n - \delta s)exp(\alpha_n L_a - \delta_n L_a)}{\delta_n - \delta s}}$ and

$D_n = -\frac{(\alpha_n - \delta s)exp(\alpha_n L_a - \delta_n L_a)}{\delta_n - \delta s} N_n$.

Conducting Laplace transform to Eqs. (1c) - (1d), Eq. (3) and Eq. (4b), yields

$$D_{uz} \frac{\partial^2 \bar{C}_{um}}{\partial z^2} + D_{ux} \frac{\partial^2 \bar{C}_{um}}{\partial x^2} - v_z \frac{\partial \bar{C}_{um}}{\partial z} - E_2 \bar{C}_{um} = 0, \ b_1 \le z < b_1 + b_2, 0 \le x \le L_a, \quad \text{(A9)}$$

$$\bar{C}_{uim} = \frac{\varepsilon_u/\theta_{uim}}{\varepsilon_u/\theta_{uim} + \lambda_{uim} + R_{uim} s} \bar{C}_{um}, \ b_1 \le z < b_1 + b_2, 0 \le x \le L_a, \quad \text{(A10)}$$

$$\bar{C}_{um}(x, z, s)|_{z=b_1+b_2} = 0, \ 0 \le x \le L_a, \quad \text{(A11)}$$

$$\bar{C}_{um}(x, z, s)|_{z=b_1} = \bar{C}_m(x, z, s)|_{z=b_1}, \ 0 \le x \le L_a, \quad \text{(A12)}$$

$$\theta_{um} \left[v_z \bar{C}_{um}(x, z, s) - D_{uz} \frac{\partial \bar{C}_{um}(x,z,s)}{\partial z} \right]\Big|_{z=b_1} = -\left[\theta_m D_z \frac{\partial \bar{C}_m(x,z,s)}{\partial z} \right]\Big|_{z=b_1}, \ 0 \le x \le L_a, \quad \text{(A13)}$$

where $E_2 = \lambda_{um} + sR_{um} + \varepsilon_u/\theta_{um} - \frac{\varepsilon_u^2/\theta_{um}\theta_{uim}}{\varepsilon_u\theta_{uim} + \lambda_{uim} + R_{uim} s}$.

Assuming (Rezaei et al., 2016)

$$\bar{C}_{\mathrm{um}} = \sum_{\mathrm{n}=0}^{\infty}[\mathrm{N_n}exp(\alpha_{\mathrm{n}}x) + \mathrm{D_n}exp(\delta_{\mathrm{n}}x)] \times F_1, \quad \text{(A14)}$$

where F_1 depends on the z coordinate only. Substituting Eq. (A14) into Eq. (A9) yields

$$D_{\mathrm{uz}}\frac{\partial^2 F_1}{\partial z^2} - v_z\frac{\partial F_1}{\partial z} - (E_2 + D_{\mathrm{ux}}\alpha_{\mathrm{n}}^2)F_1 = 0,\ b_1 \le z < b_1 + b_2,\ 0 \le x \le L_{\mathrm{a}}, \quad \text{(A15)}$$

The general solution of Eq. (A15) is

$$F_1 = \mathrm{A_n}exp(\beta_{\mathrm{n}}z) + \mathrm{B_n}exp(\sigma_{\mathrm{n}}z), \quad \text{(A16)}$$

where $\mathrm{A_n}$ and $\mathrm{B_n}$ are constant, $\beta_{\mathrm{n}} = \frac{v_z - \sqrt{v_z^2 + 4D_{\mathrm{uz}}(E_2 + D_{\mathrm{ux}}\alpha_{\mathrm{n}}^2)}}{2D_{\mathrm{uz}}}$ and $\sigma_{\mathrm{n}} = \frac{v_z + \sqrt{v_z^2 + 4D_{\mathrm{uz}}(E_2 + D_{\mathrm{ux}}\alpha_{\mathrm{n}}^2)}}{2D_{\mathrm{uz}}}$.

The general solution of Eq. (A9) is

$$\bar{C}_{\mathrm{um}} = \sum_{\mathrm{n}=0}^{\infty}[\mathrm{A_n}exp(\beta_{\mathrm{n}}z) + \mathrm{B_n}exp(\sigma_{\mathrm{n}}z)] \times [\mathrm{N_n}exp(\alpha_{\mathrm{n}}x) + \mathrm{D_n}exp(\delta_{\mathrm{n}}x)]. \quad \text{(A17)}$$

According to the boundary conditions of Eqs. (A11) - (A12), the coefficients of $\mathrm{A_n}$ and $\mathrm{B_n}$ could be obtained, yields

$$\mathrm{A_n} = -\frac{cos(\omega_{\mathrm{n}}b_1)exp[\sigma_{\mathrm{n}}(b_1+b_2)-\beta_{\mathrm{n}}(b_1+b_2)]}{exp[\sigma_{\mathrm{n}}b_1]-exp[\sigma_{\mathrm{n}}(b_1+b_2)-\beta_{\mathrm{n}}b_2]} \text{ and } \mathrm{B_n} = \frac{cos(\omega_{\mathrm{n}}b_1)}{exp[\sigma_{\mathrm{n}}b_1]-exp[\sigma_{\mathrm{n}}(b_1+b_2)-\beta_{\mathrm{n}}b_2]}.$$

According to Eq. (A13), one has

$$\omega_{\mathrm{n}}tan(\omega_{\mathrm{n}}b_1) = \frac{W_1[v_z exp(\beta_{\mathrm{n}}b_1)-D_{\mathrm{uz}}\beta_{\mathrm{n}}exp(\beta_{\mathrm{n}}b_1)]}{D_z} + \frac{W_2[v_z exp(\sigma_{\mathrm{n}}b_1)+D_{\mathrm{uz}}\sigma_{\mathrm{n}}exp(\sigma_{\mathrm{n}}b_1)]}{D_z}, \quad \text{(A18)}$$

where $W_1 = -\frac{\theta_{\mathrm{um}}}{\theta_{\mathrm{m}}}\frac{exp[\sigma_{\mathrm{n}}(b_1+b_2)-\beta_{\mathrm{n}}(b_1+b_2)]}{exp[\sigma_{\mathrm{n}}b_1]-exp[\sigma_{\mathrm{n}}(b_1+b_2)-\beta_{\mathrm{n}}b_2]}$ and $W_2 = \frac{\theta_{\mathrm{um}}/\theta_{\mathrm{m}}}{exp[\sigma_{\mathrm{n}}b_1]-exp[\sigma_{\mathrm{n}}(b_1+b_2)-\beta_{\mathrm{n}}b_2]}$.

Appendix B. The finite-difference solution

In numerical modeling, the horizontal spatial domain of the aquifer-aquitard system $[0, L_{\mathrm{a}}]$ is uniformly discretized into N subdomains (e.g., cells) with $N+1$ nodes, and one has

$$x_i = \frac{x_{i+1/2} - x_{i-1/2}}{2},\ i = 1, 2, \ldots, N, \quad \text{(B1)}$$

where $x_{i+1/2}$ is

$$x_{i+1/2} = i\frac{L_a}{N},\ i = 1, 2, \dots, N. \quad \text{(B2)}$$

The aquifer and aquitard are vertically discretized into $M_1 - 1$ and $M_2 - 1$ subdomains, respectively, and one has

$$z_j = \frac{z_{j+1/2} - z_{j-1/2}}{2},\ j = 1, 2, \dots, M_1, \quad \text{(B3a)}$$

$$z_k = \frac{z_{k+1/2} - z_{k-1/2}}{2},\ k = 1, 2, \dots, M_2, \quad \text{(B3b)}$$

where $z_{j+1/2}$ and $z_{k+1/2}$ are

$$z_{j+1/2} = j\frac{b_1}{M_1},\ j = 1, 2, \dots, M_1, \quad \text{(B4a)}$$

$$z_{k+1/2} = k\frac{b_2}{M_2},\ k = 1, 2, \dots, M_2. \quad \text{(B4b)}$$

The finite-difference schemes of Eqs. (1a) - (1d) are

$$\frac{\partial C_{\mathrm{m},i,j}}{\partial t} =$$

$$\frac{\frac{D_x}{R_\mathrm{m}}\frac{C_{\mathrm{m},i-1,j} - C_{\mathrm{m},i,j}}{x_i - x_{i-1}} - \frac{D_x}{R_\mathrm{m}}\frac{C_{\mathrm{m},i,j} - C_{\mathrm{m},i+1,j}}{x_{i+1} - x_i}}{x_{i+1/2} - x_{i-1/2}} + \frac{\frac{D_z}{R_\mathrm{m}}\frac{C_{\mathrm{m},i,j-1} - C_{m,i,j}}{z_j - z_{j-1}} - \frac{D_z}{R_\mathrm{m}}\frac{C_{\mathrm{m},i,j} - C_{\mathrm{m},i,j+1}}{z_{j+1} - z_j}}{z_{j+1/2} - z_{j-1/2}} - \frac{v_x}{R_\mathrm{m}}\frac{C_{\mathrm{m},i+\frac{1}{2},j} - C_{\mathrm{m},i-\frac{1}{2},j}}{x_{i+\frac{1}{2}} - x_{i-\frac{1}{2}}} - \left(\frac{\lambda_\mathrm{m}}{R_\mathrm{m}} + \right.$$

$$\left.\frac{\varepsilon}{\theta_\mathrm{m} R_\mathrm{m}}\right) C_{\mathrm{m},i,j} + \frac{\varepsilon}{\theta_\mathrm{m} R_\mathrm{m}} C_{\mathrm{im},i,j},\ i = 1, 2, \dots, N,\ j = 1, 2, \dots, M_1, \quad \text{(B5a)}$$

$$\frac{\partial C_{\mathrm{im},i,j}}{\partial t} = \frac{\varepsilon}{\theta_\mathrm{im} R_\mathrm{im}} C_{\mathrm{m},i,j} - \left(\frac{\varepsilon}{\theta_\mathrm{im} R_\mathrm{im}} + \frac{\lambda_\mathrm{im}}{R_\mathrm{im}}\right) C_{\mathrm{im},i,j},\ i = 1, 2, \dots, N,\ j = 1, 2, \dots, M_1, \quad \text{(B5b)}$$

$$\frac{\partial C_{\mathrm{um},i,k}}{\partial t} = \frac{\frac{D_{\mathrm{uz}}}{R_\mathrm{um}}\frac{C_{\mathrm{um},i,k-1} - C_{\mathrm{um},i,k}}{z_k - z_{k-1}} - \frac{D_{uz}}{R_\mathrm{um}}\frac{C_{\mathrm{um},i,k} - C_{\mathrm{um},i,k+1}}{z_{k+1} - z_k}}{z_{k+1/2} - z_{k-1/2}} + \frac{\frac{D_{\mathrm{ux}}}{R_\mathrm{um}}\frac{C_{\mathrm{um},i,k-1} - C_{\mathrm{um},i,k}}{x_i - x_{i-1}} - \frac{D_{\mathrm{ux}}}{R_\mathrm{um}}\frac{C_{\mathrm{um},i,k} - C_{\mathrm{um},i,k+1}}{x_{i+1} - x_i}}{x_{i+1/2} - x_{i-1/2}} -$$

$$\frac{v_z}{R_\mathrm{um}}\frac{C_{\mathrm{um},i,k+\frac{1}{2}} - C_{\mathrm{um},i,k-\frac{1}{2}}}{z_{k+\frac{1}{2}} - z_{k-\frac{1}{2}}} - \left(\frac{\lambda_\mathrm{um}}{R_\mathrm{um}} + \frac{\varepsilon_u}{\theta_\mathrm{um} R_{um}}\right) C_{um,i,k} - \frac{\varepsilon_u}{\theta_\mathrm{um} R_{um}} C_{\mathrm{uim},i,k},\ i = 1, 2, \dots, N,\ k =$$

$$1, 2, \dots, M_2, \quad \text{(B5c)}$$

$$\frac{\partial C_{\mathrm{uim},i,k}}{\partial t} = \frac{\varepsilon_\mathrm{u} C_{\mathrm{um},i,k}}{\theta_\mathrm{uim} R_\mathrm{uim}} - \left(\frac{\varepsilon_\mathrm{u}}{\theta_\mathrm{uim} R_\mathrm{uim}} + \frac{\lambda_\mathrm{uim}}{R_\mathrm{uim}}\right) C_{\mathrm{uim},i,k},\ i = 1, 2, \dots, N\ ,k = 1, 2, \dots, M_2, \quad \text{(B5d)}$$

where $C_{\mathrm{m},i,j}$ and $C_{\mathrm{im},i,j}$ are the concentrations of mobile zone and immobile zone in the aquifer at node (i,j), respectively; $C_{\mathrm{um},i,k}$ and $C_{\mathrm{uim},i,k}$ are the concentrations of mobile zone and immobile zone in the aquitard at node (i,j), respectively.

References

Baeumer, B., Benson, D.A., Meerschaert, M.M., Wheatcraft, S.W., 2001. Subordinated advection - dispersion equation for contaminant transport. Water Resources Research, 37(6): 1543-1550.

Barbour, S.L., Hendry, M.J., Wassenaar, L.I., 2012. In situ experiment to determine advective-diffusive controls on solute transport in a clay-rich aquitard. Journal of Contaminant Hydrology, 131(1-4): 79-88.

Chen, C.S., 1985. Analytical and approximate solutions to radial dispersion from an injection well to a geological unit with simultaneous diffusion into adjacent strata. Water Resources Research, 21(8): 1069-1076.

Chen, J.-S., Ho, Y.-C., Liang, C.-P., Wang, S.-W., Liu, C.-W., 2018. Analytical model for coupled multispecies advective dispersive transport subject to rate-limited sorption. Hydrology and Earth System Sciences Discussions: 1-45.

Chen, K., Zhan, H., 2018. A Green's function method for two-dimensional reactive solute transport in a parallel fracture-matrix system. Journal of Contaminant Hydrology, 213(2018): 15-21.

Chen, K., Zhan, H., Yang, Q., 2017. Fractional Models Simulating Non - Fickian Behavior in Four - Stage Single - Well Push - Pull Tests. Water Resources Research, 53(11): 9528-9545.

582 Dubner, H., Abate, J., 1968. Numerical Inversion of Laplace Transforms by Relating Them
583 to the Finite Fourier Cosine Transform. Journal of the Acm, 15(1): 115-123.
584 Fujikawa, Y., Fukui, M., 1990. Adsorptive solute transport in fractured rock: analytical
585 solutions for delta-type source conditions. Journal of Contaminant Hydrology, 6(1): 85-102.
586 Guerrero, A., Cherry, J.A., Rudolph, D.L., 1993. Large‐Scale Aquitard Consolidation Near
587 Mexico City. Groundwater, 31(5): 708-718.
588 Hansen, S.K., Vesselinov, V.V., Reimus, P.W., Lu, Z., 2017. Inferring subsurface
589 heterogeneity from push-drift tracer tests. Water Resources Research, 53(7): 6322-6329.
590 Hendry, M.J., Kelln, C.J., Wassenaar, L.I., Shaw, J., 2004. Characterizing the hydrogeology
591 of a complex clay-rich aquitard system using detailed vertical profiles of the stable isotopes of
592 water. Journal of Hydrology, 293(1-4): 47-56.
593 Kookana, R.S., Aylmore, L., Gerritse, R., 1992. Time-dependent sorption of pesticides
594 during transport in soils. Soil science, 154(3): 214-225.
595 Li, X., Wen, Z., Zhan, H., Wu, F., Zhu, Q., 2021. Laboratory observations for two-
596 dimensional solute transport in an aquifer-aquitard system. Environmental Science and Pollution
597 Research, 4(2021): 1-15.
598 Lin, Z., Puls, R.W., 2000. Adsorption, desorption and oxidation of arsenic affected by clay
599 minerals and aging process. Environmental Geology, 39(7): 753-759.
600 Liu, C.-T., Yeh, H.-D., Yeh, L.-M., 2013. Modeling contaminant transport in a two-aquifer
601 system with an intervening aquitard. Journal of Hydrology, 499(2013): 200-209.
602 Mazurek, M. et al., 2011. Natural tracer profiles across argillaceous formations. Applied
603 Geochemistry, 26(7): 1035-1064.

Moriasi, D.N. et al., 2007. Model evaluation guidelines for systematic quantification of accuracy in watershed simulations. Transactions of the ASABE, 50(3): 885-900.

Morris, M.D., 1991. Factorial Sampling Plans for Preliminary Computational Experiments. Technometrics, 33(2): 161-174.

Rezaei, A., Zare, M., Zhan, H., 2016. Aquitard Horizontal Dispersion on Reactive Solute Transport in an Aquifer–Aquitard System. Transport in Porous Media, 113(3): 695-716.

Rezaei, A., Zhan, H., Zare, M., 2013. Impact of thin aquitards on two-dimensional solute transport in an aquifer. Journal of Contaminant Hydrology, 152(2013): 117-136.

Rezanezhad, F. et al., 2017. The Role of Pore Structure on Nitrate Reduction in Peat Soil: A Physical Characterization of Pore Distribution and Solute Transport. Wetlands, 37: 951-960.

Rezanezhad, F. et al., 2016. Structure of peat soils and implications for water storage, flow and solute transport: A review update for geochemists. Chemical Geology, 429: 75-84.

Roubinet, D., de Dreuzy, J.R., Tartakovsky, D.M., 2012. Semi-analytical solutions for solute transport and exchange in fractured porous media. Water Resources Research, 48(1): W01542.

Saltelli, A. et al., 2008. Global sensitivity analysis: the primer. John Wiley & Sons.

Sathyanarayanamurthy, H., Chinnam, R.B., 2009. Metamodels for variable importance decomposition with applications to probabilistic engineering design. Computers & Industrial Engineering, 57(3): 996-1007.

Schapery, R.A., 1962. Approximate Methods of Transform Inversion for Viscoelastic Stress Analysis. Proc Fourth USNat Congr Appl Mech, 2(1962):1075.

Shampine, L.F., Reichelt, M.W., 1997. The matlab ode suite. SIAM journal on scientific computing, 18(1): 1-22.

626 Singh, M.K., Singh, R.K., Pasupuleti, S., 2020. Study of forward–backward solute
627 dispersion profiles in a semi-infinite groundwater system. Hydrological Sciences Journal, 65(8):
628 1416-1429.
629 Starr, R., Gillham, R., Sudicky, E., 1985. Experimental investigation of solute transport in
630 stratified porous media: 2. The reactive case. Water Resources Research, 21(7): 1043-1050.
631 Stehfest, Harald, 1970a. Algorithm 368: Numerical inversion of Laplace transforms [D5].
632 Communications of the Acm, 13(1): 47-49.
633 Stehfest, Harald, 1970b. Remark on algorithm 368: Numerical inversion of Laplace
634 transforms. Communications of the Acm, 13(10): 624.
635 Sudicky, E., Frind, E., 1982. Contaminant transport in fractured porous media: Analytical
636 solutions for a system of parallel fractures. Water Resources Research, 18(6): 1634-1642.
637 Sudicky, E.A., Gillham, R.W., Frind, E.O., 1985. Experimental Investigation of Solute
638 Transport in Stratified Porous Media: 1. The Nonreactive Case. Water Resources Research,
639 21(7): 1043-1050.
640 Tang, D.H., Frind, E.O., Sudicky, E.A., 1981. Contaminant transport in fractured porous
641 media: Analytical solution for a single fracture. Water Resources Research, 17(3): 555-564.
642 Tang, Y., Aral, M.M., 1992. Contaminant transport in layered porous media: 1. General
643 solution. Water Resources Research, 28(5): 1389-1397.
644 Tiscareno-Lopez, M., Lopes, V., Stone, J., Lane, L., 1993. Sensitivity analysis of the WEPP
645 watershed model for rangeland applications I: Hillslope processes. Transactions of the ASAE,
646 36(6): 1659-1672.
647 Van Genuchten, M.T., 1985. Convective-dispersive transport of solutes involved in
648 sequential first-order decay reactions. Computers & Geosciences, 11(2): 129-147.

649 Wang, Q., Gu, H., Zhan, H., Shi, W., Zhou, R., 2019. Mixing Effect on Reactive Transport
650 in a Column with Scale Dependent Dispersion. Journal of Hydrology, 582(6): 124494.
651 Wang, Q., Shi, W., Zhan, H., Xiao, X., 2020a. New model of Single-Well Push-Pull thermal
652 test in a Fracture-Matrix system. Journal of Hydrology, 585(2020): 124807.
653 Wang, Q., Wang, J., Zhan, H., Shi, W., 2020b. New model of reactive transport in a single-
654 well push–pull test with aquitard effect and wellbore storage. Hydrology and Earth System
655 Sciences, 24(8): 3983-4000.
656 Wang, Q., Zhan, H., 2013. Radial reactive solute transport in an aquifer–aquitard system.
657 Advances in Water Resources, 61(2013): 51-61.
658 Xao, C., Teng, M., Yao, D., 2020. Arsenic releasing mechanisms during clayey sediments
659 compaction: An experiment study. Journal of Hydrology, 597(2020):125743.
660 Yang, M., Annable, M.D., Jawitz, J.W., 2016. Solute source depletion control of forward
661 and back diffusion through low-permeability zones. Journal of contaminant hydrology,
662 193(2016): 54-62.
663 Yeh, G.T., 2000. Numerical Methods for Advection-Dominant Transport. Computational
664 Subsurface Hydrology, pp. 93-198. Springer, Boston, MA.
665 Zhan, H., Wen, Z., Gao, G., 2009a. An analytical solution of two-dimensional reactive
666 solute transport in an aquifer-aquitard system. Water Resources Research, 45(10): W10501.
667 Zhan, H., Wen, Z., Huang, G., Sun, D., 2009b. Analytical solution of two-dimensional
668 solute transport in an aquifer–aquitard system. Journal of Contaminant Hydrology, 107(3-4):
669 162-174.

Zheng, C., Wang, P., 1999. MT3DMS: A modular 3-D multispecies model for simulation of advection dispersion and chemical reactions of contaminants in groundwater systems. Rep., Army Engineer Research and Development Center, Vicksburg, Mississippi; 1999.

Zhou, R., Zhan, H., 2018. Reactive solute transport in an asymmetrical fracture–rock matrix system. Advances in Water Resources, 112(2018): 224-234.

Zhou, R., Zhan, H., Chen, K., 2017. Reactive solute transport in a filled single fracture-matrix system under unilateral and radial flows. Advances in Water Resources, 104(2017): 183-194.

Zhu, Y., Zhan, H., 2018. Quantification of solute penetration in an asymmetric fracture-matrix system. Journal of Hydrology, 563(2018): 586-598.

680 ## Table Caption

681 **Table 1.** The values of RSR caused by the models of this study and Li's model.

682 **Table 2.** Parameter range used in the global sensitivity analysis.

683

684 ## Figure Caption

685 **Figure 1.** Schematic diagram of 2D reactive transport in an aquifer-aquitard system in the
686 laboratory-controlled experiment.

687 **Figure 2.** Comparison between the numerical and analytical solutions. (a) C_{m}/C_0 V.S. t at
688 different z; (b) C_{m}/C_0 V.S. z at different x. "ANA" represents the curves produced by the
689 analytical model of this study.

690 **Figure 3.** Fitness of observed BTCs for different locations in the aquifer. (a) Observation points
691 of (41), (43) and (45); (b) Observation points of (51), (53) and (55).

692 **Figure 4.** Fitness of observed BTCs for different locations in the aquitard. (a) Observation points
693 of (31), (21) and (11); (b) Observation points of (32), (22) and (12); (c) Observation points of
694 (33), (23) and (13); (d) Observation points of (34), (24) and (14); (e) Observation points of (35),
695 (25) and (1); (f) Observation points of (36), (26) and (16).

696 **Figure 5.** The comparison of BTCs between the new analytical models and Li's model. (a)
697 Observation points (41), (43) and (45); (b) Observation points (51), (53) and (55).

698 **Figure 6.** BTCs for different V_{in} and z.

699 **Figure 7.** RTDs for different V_{in} and z.

700 **Figure 8.** MF variation crossing the aquifer-aquitard interface along the x- direction for
701 different times.

Figure 9. Contributions of the diffusion, dispersion, and advection in aquitard on the aquifer-aquitard interface MF at $t = 5.5$h.

Figure 10. Sensitivity analysis of the input parameters on the output concentration at z =0.16m and x =0.10m. (a) Variation in μ_i^* with time; (b) Variation in σ_i with time.

Figures

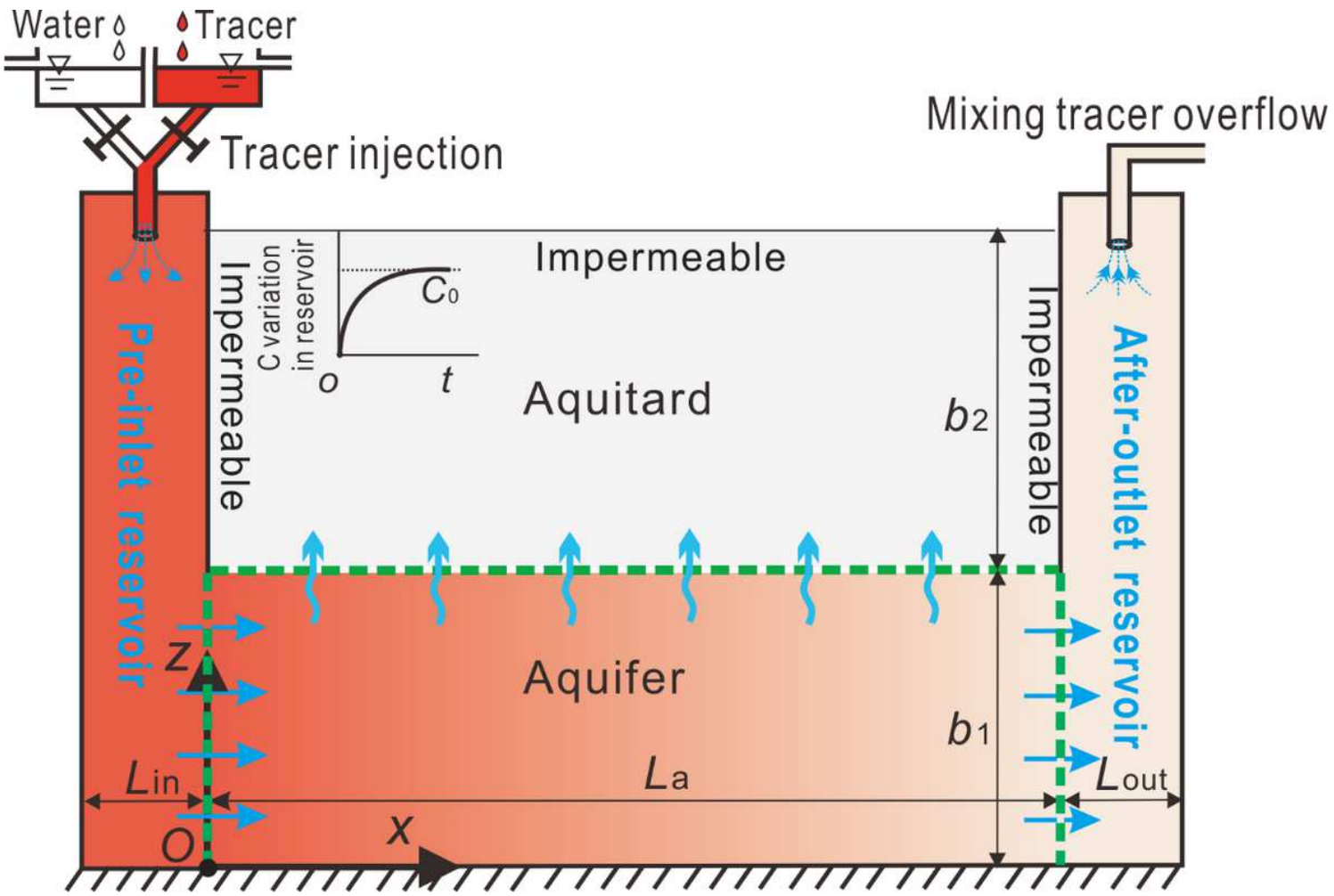

Figure 1

Schematic diagram of 2D reactive transport in an aquifer-aquitard system in the laboratory-controlled experiment.

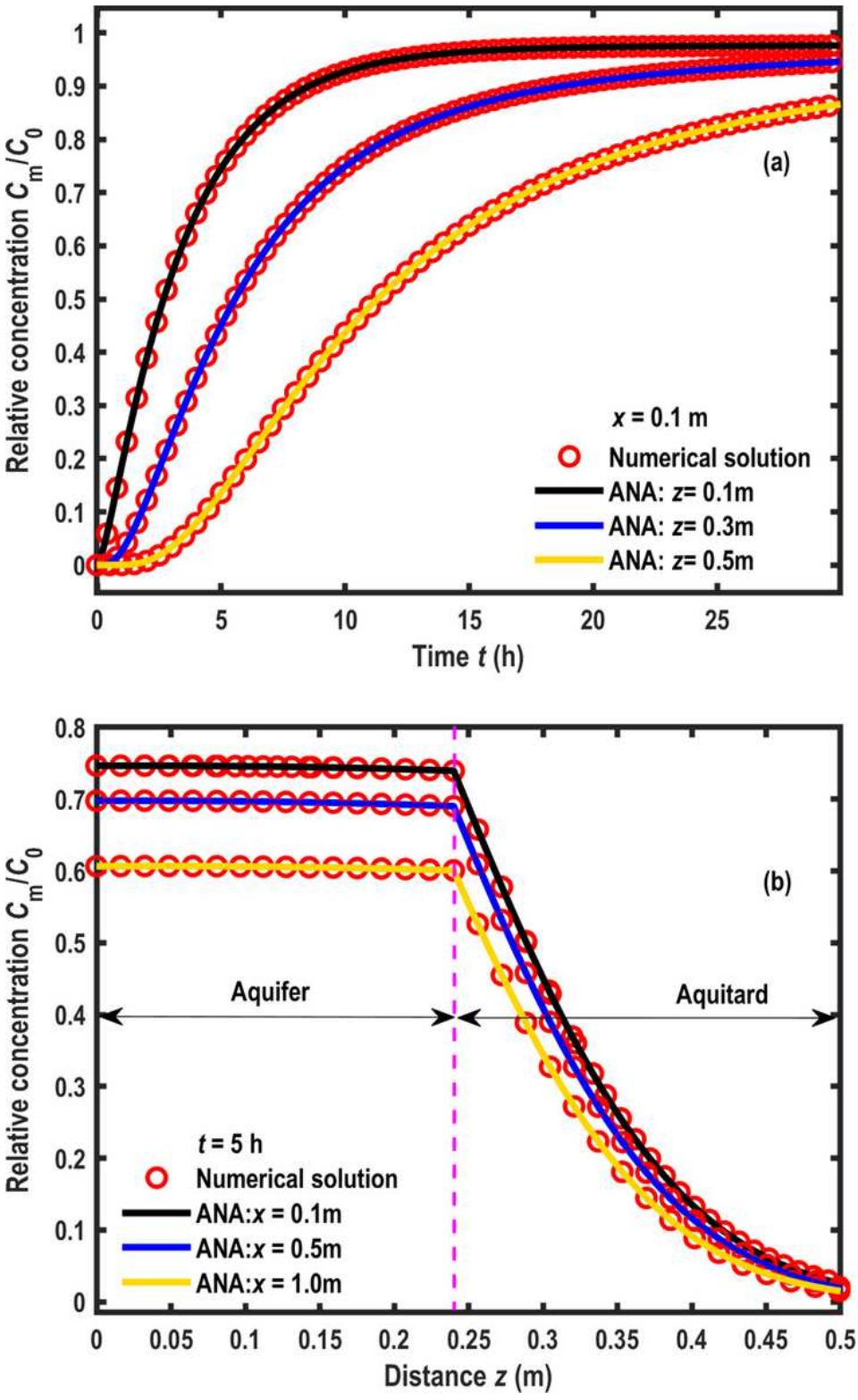

Figure 2

Comparison between the numerical and analytical solutions. (a) V.S. at different ; (b) V.S. at different . "ANA" represents the curves produced by the analytical model of this study.

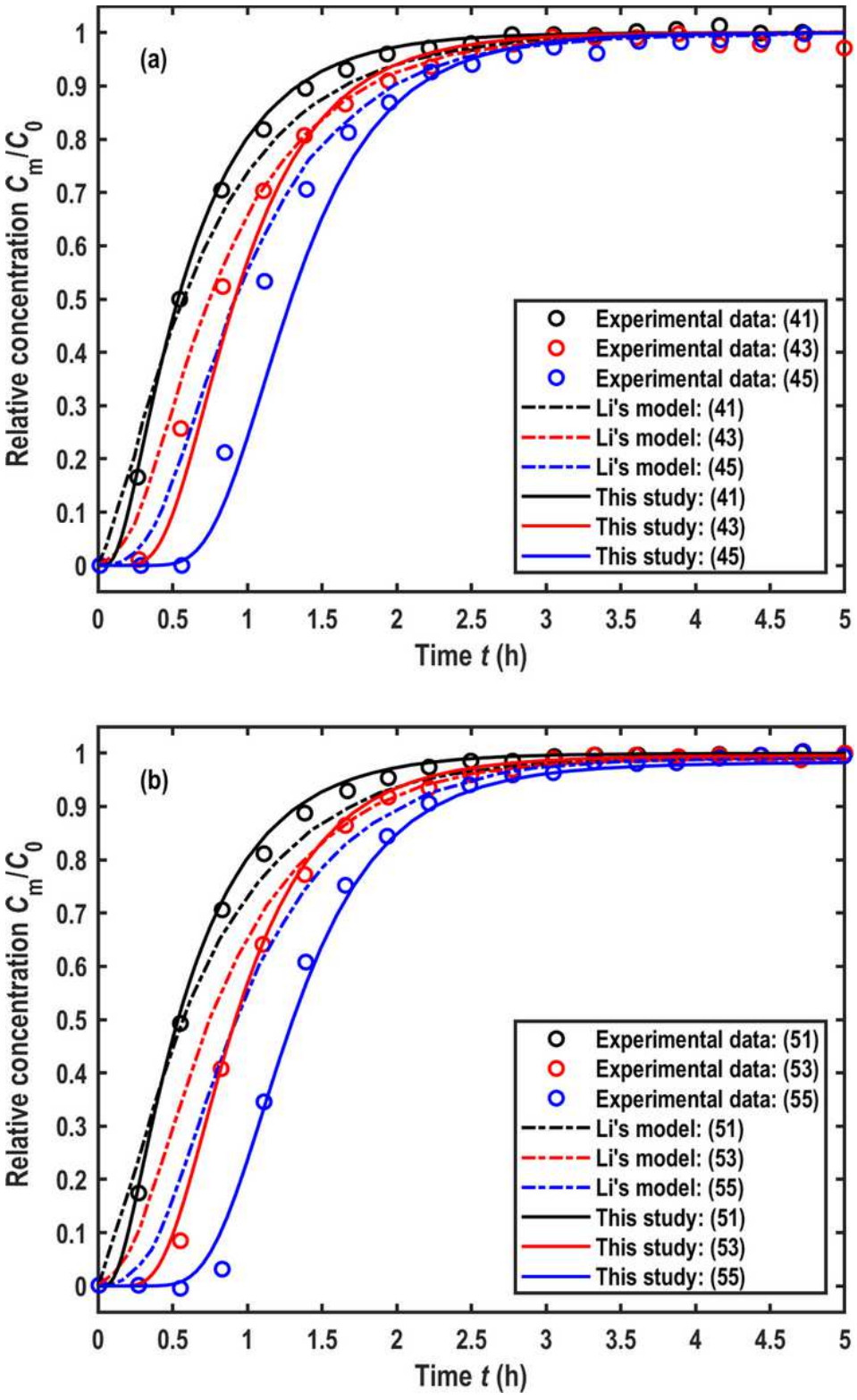

Figure 3

Fitness of observed BTCs for different locations in the aquifer. (a) Observation points of (41), (43) and (45); (b) Observation points of (51), (53) and (55).

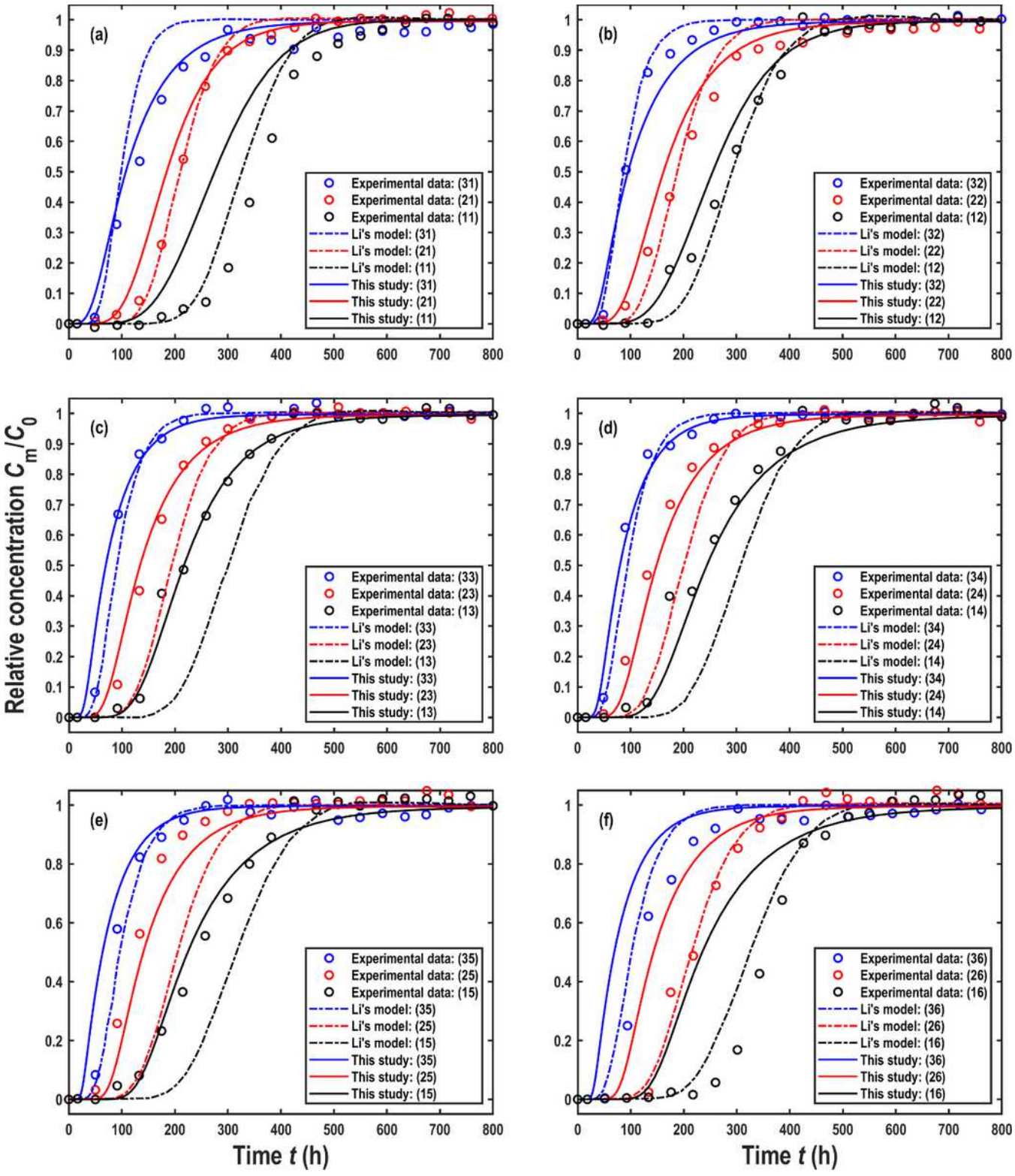

Figure 4

Fitness of observed BTCs for different locations in the aquitard. (a) Observation points of (31), (21) and (11); (b) Observation points of (32), (22) and (12); (c) Observation points of (33), (23) and (13); (d) Observation points of (34), (24) and (14); (e) Observation points of (35), (25) and (1); (f) Observation points of (36), (26) and (16).

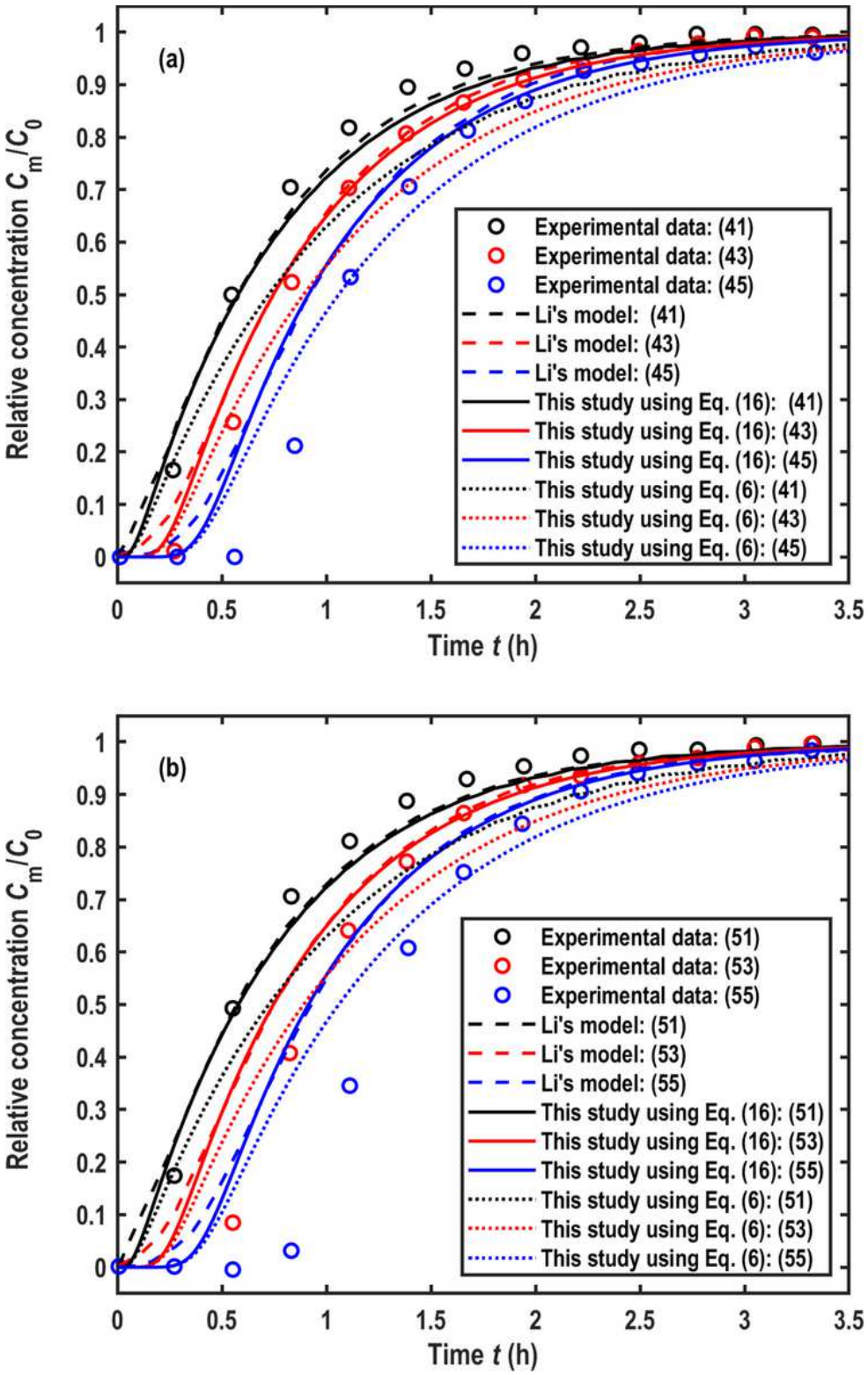

Figure 5

The comparison of BTCs between the new analytical models and Li's model. (a) Observation points (41), (43) and (45); (b) Observation points (51), (53) and (55).

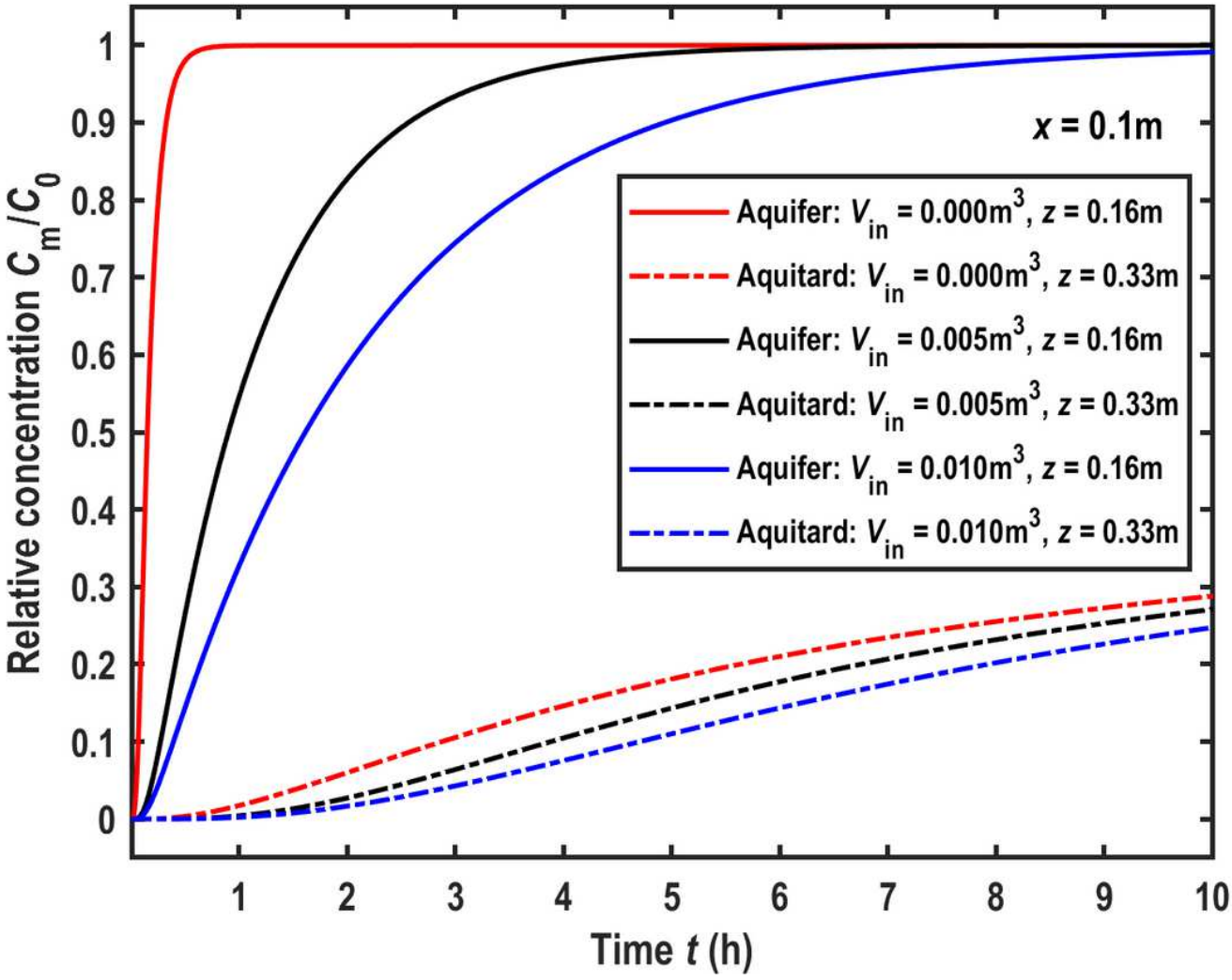

Figure 6

BTCs for different *Vin* and *z*.

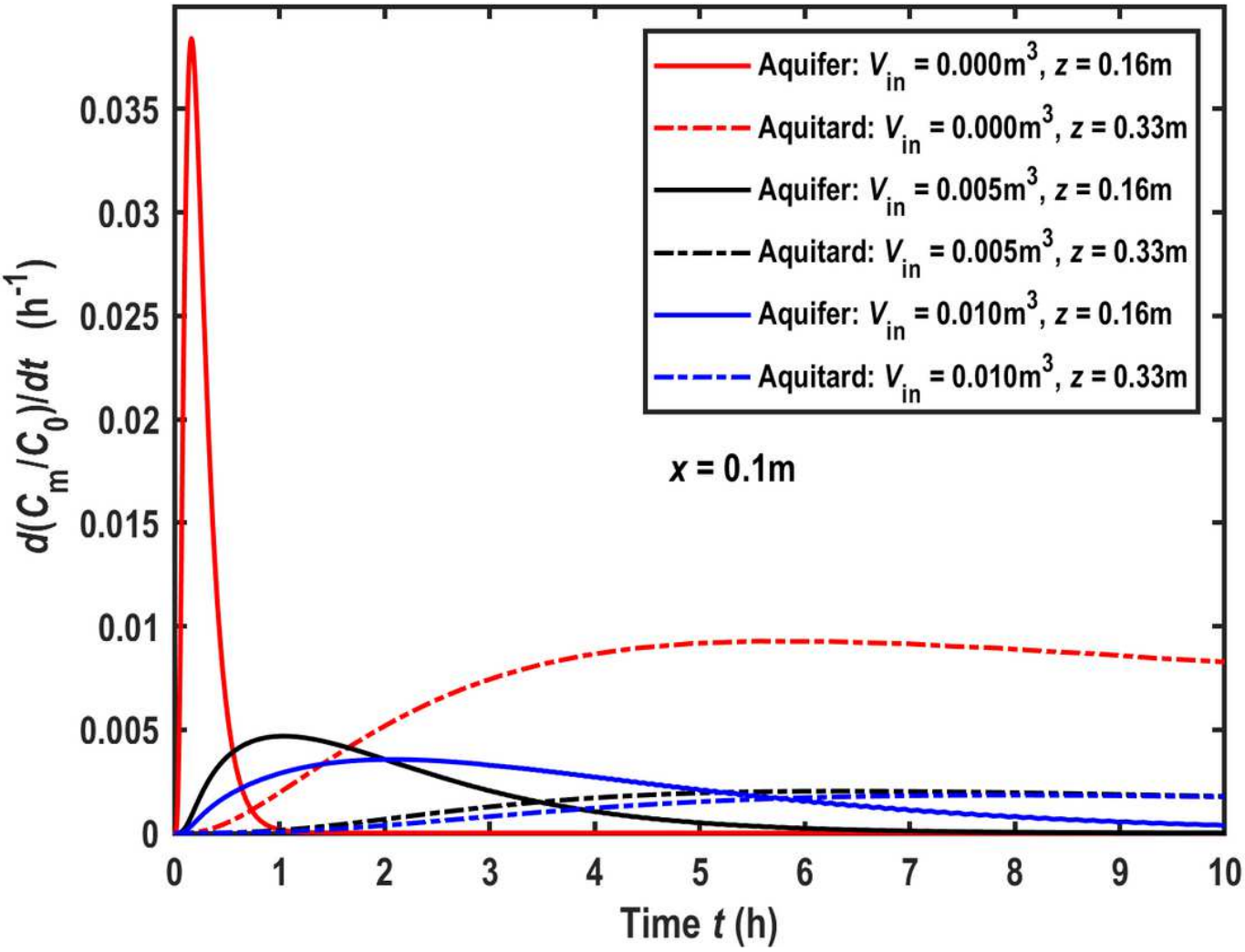

Figure 7

RTDs for different *Vin* and *z*.

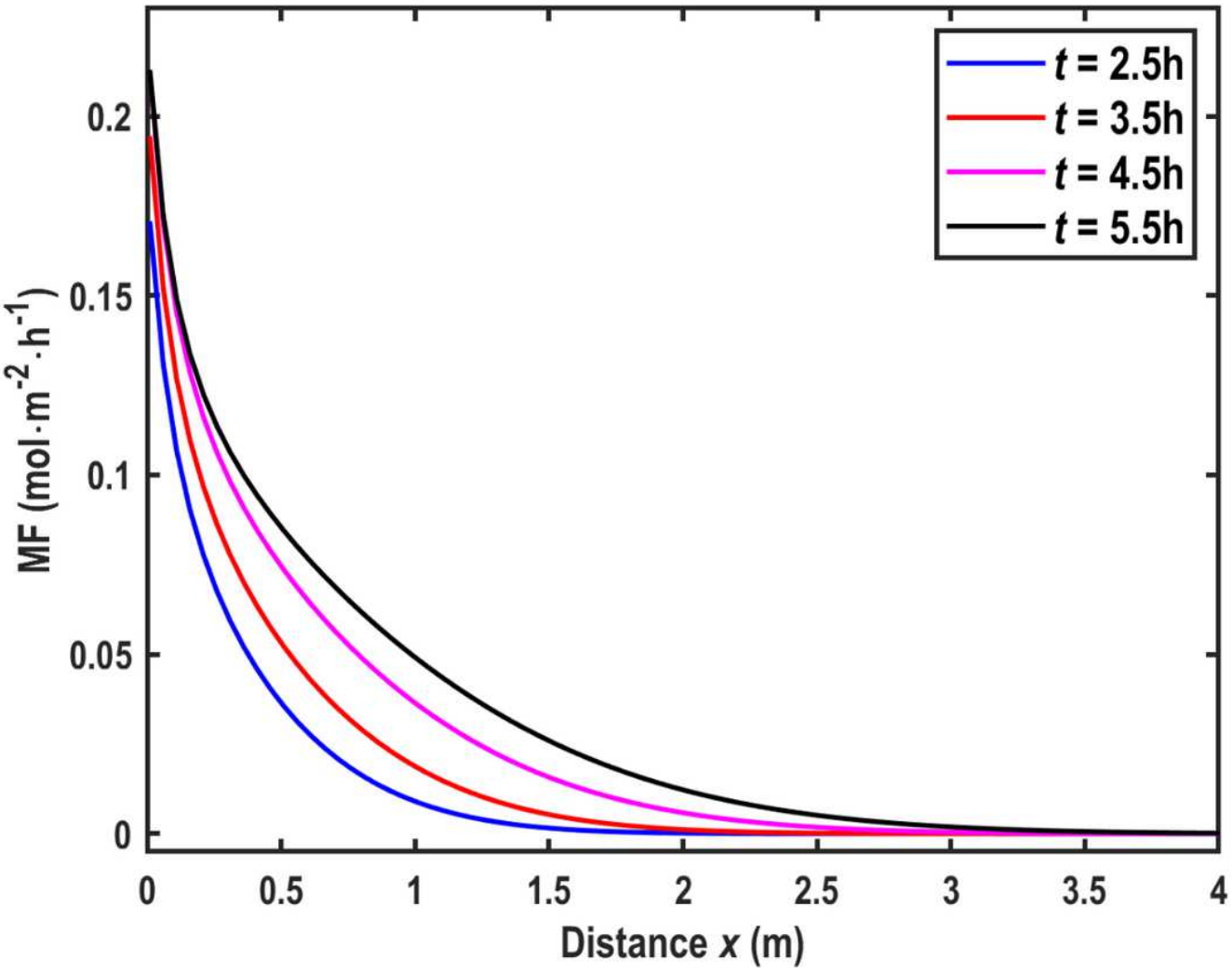

Figure 8

MF variation crossing the aquifer-aquitard interface along the *x*- direction for different times.

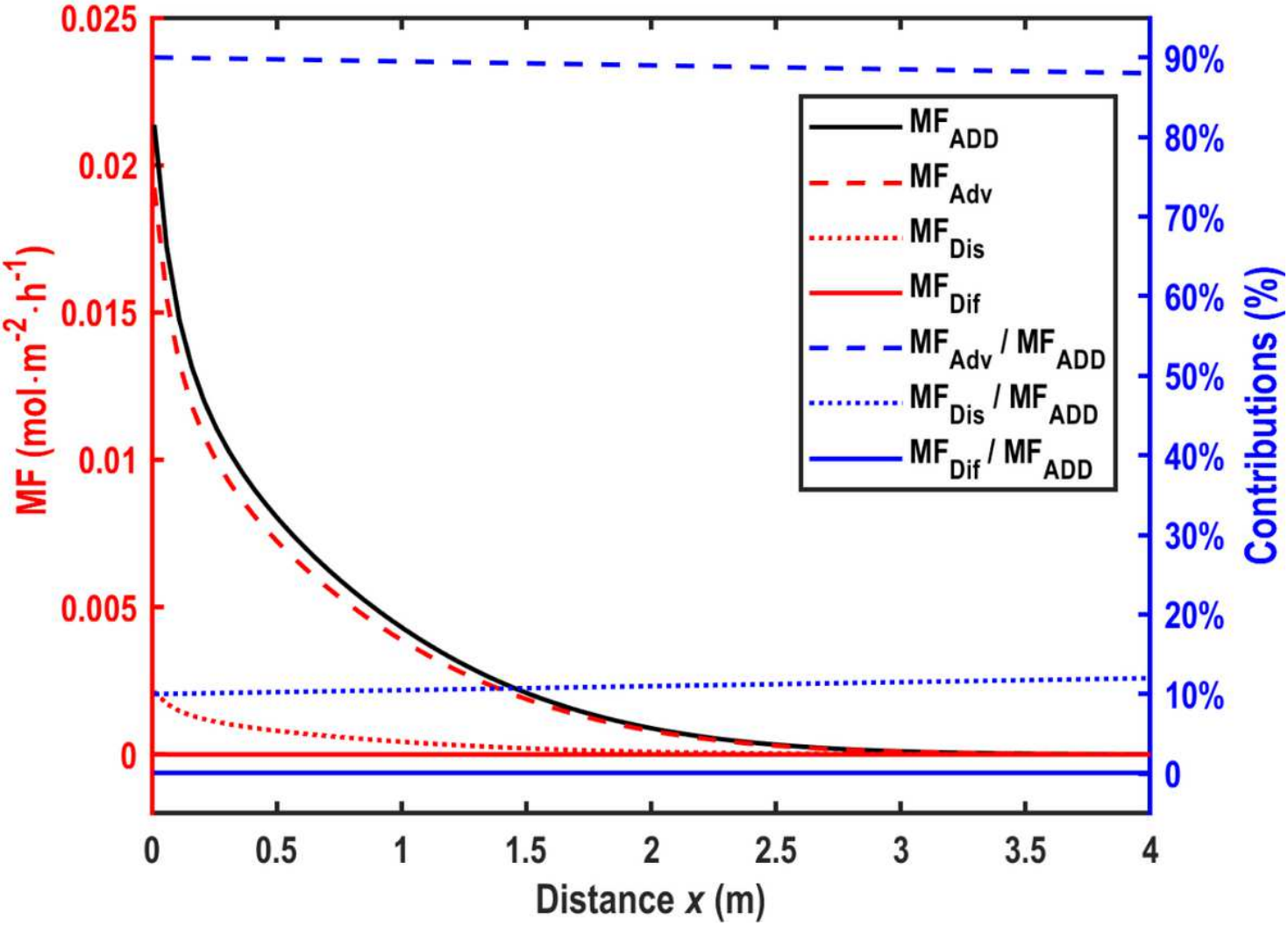

Figure 9

Contributions of the diffusion, dispersion, and advection in aquitard on the aquifer-aquitard interface MF at t = 5.5h.

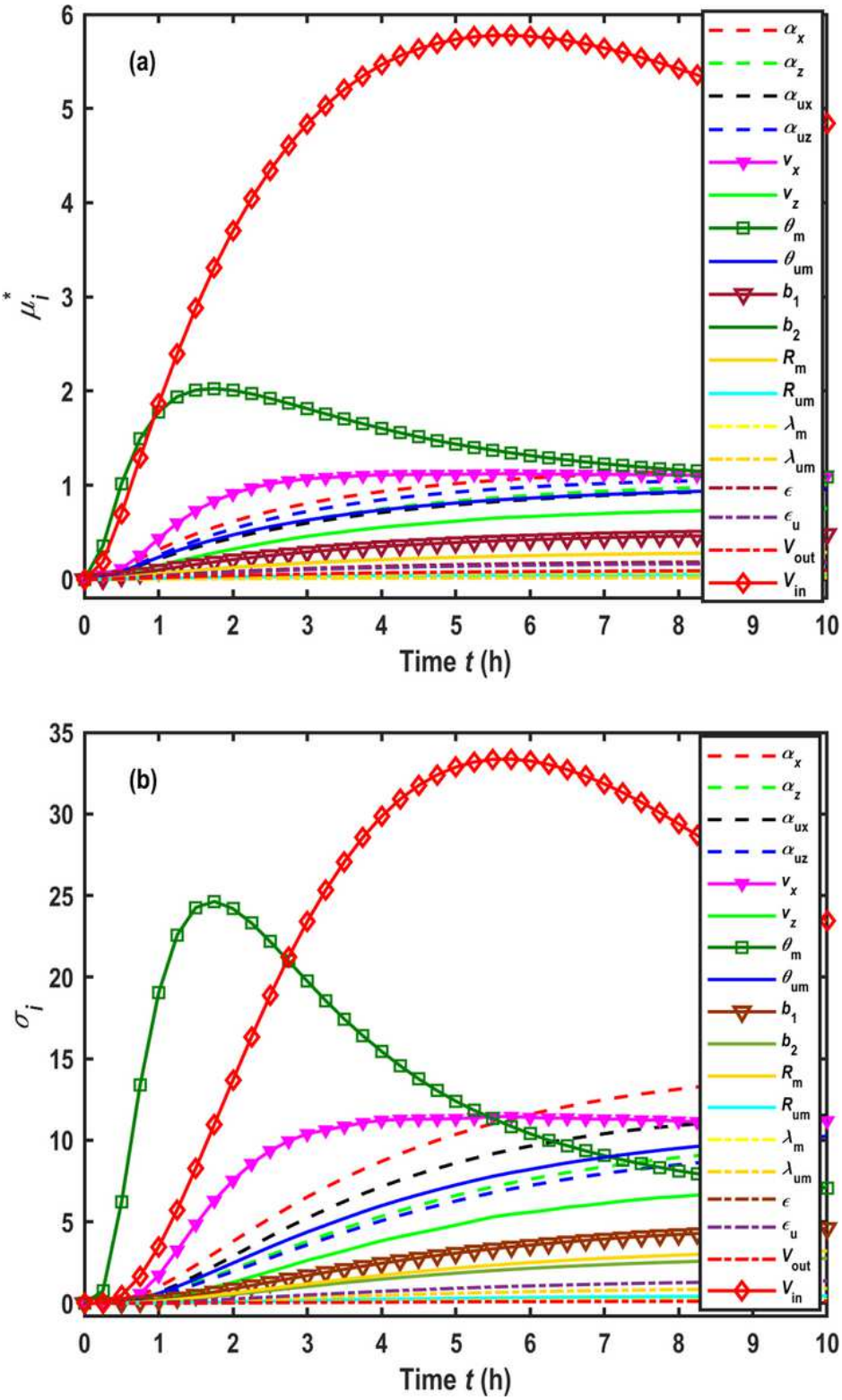

Figure 10

Sensitivity analysis of the input parameters on the output concentration at z = 0.16m and x = 0.10m. (a) Variation in μi^* with time; (b) Variation in σi with time.